



This is to certify that the  
thesis entitled

**CLASSICAL MIXING APPROACHES TO DETERMINE  
EFFECTIVE PERMITTIVITY AND PERMEABILITY OF A  
TWO-PHASE MIXTURE**

presented by

**DANIEL STEVEN KILLIPS**

has been accepted towards fulfillment  
of the requirements for the

MS degree in ELECTRICAL ENGINEERING



Major Professor's Signature

5/3/04

Date

**LIBRARY**  
**Michigan State**  
**University**

PLACE IN RETURN BOX to remove this checkout from your record.  
TO AVOID FINES return on or before date due.  
MAY BE RECALLED with earlier due date if requested.

DATE DUE	DATE DUE	DATE DUE
AUG 20 2006 08 26 06		
SEP 15 2008		

**CLASSICAL MIXING APPROACHES TO DETERMINE EFFECTIVE  
PERMITTIVITY AND PERMEABILITY OF A TWO-PHASE MIXTURE**

By

**Daniel Steven Killips**

**A THESIS**

**Submitted to  
Michigan State University  
in partial fulfillment of the requirements  
for the degree of**

**MASTER OF SCIENCE**

**Electrical and Computer Engineering**

**2004**

## ABSTRACT

# CLASSICAL MIXING APPROACHES TO DETERMINE EFFECTIVE PERMITTIVITY AND PERMEABILITY OF A TWO-PHASE MIXTURE

By

Daniel Steven Killips

Presented in this thesis is a discussion of four classical mixing approaches to predicting the relative permittivity of a two-phase mixture. These formulations are: Maxwell Garnett, Clausius Mosotti, Bruggeman and Coherent Potential. All four of these will be discussed in close detail and then compared to actual measured data from a mixture comprised of small hexaferrite spherical particles randomly dispersed throughout a non-magnetic polymer background. A description will then be given on the accuracy of these predictions and why some work better than others.

Based on the concept of duality, the electrostatic and magnetostatic formulations obey the same conditions for a given geometry subject to appropriate boundary conditions. Therefore the mixing approaches derived for permittivity should apply just the same to permeability. These formulations are again calculated and graphed with measured data in order to show how the relative permeability of a mixture is not as easily computed as was the permittivity due to the interaction between particles that is evident in magnetism.

Finally, an application of these predictions is presented along with conclusions and future work.

To my wife Shana

## ACKNOWLEDGEMENTS

First I would like to thank all those in my life who have helped me get through the thesis writing process with what I can only hope is my sanity. Special thanks goes to Dr. Leo Kempel for giving me the opportunity to further my education and for the invaluable experience I receive. Thanks also to Dr. Edward Rothwell for his excellent teachings and his availability for questions and advice. I also wish to thank Dr. Dennis Nyquist for participating on my committee and for helping with the measurement technique.

Much appreciation goes to Dr. Steve Schneider from AFRL/SNRR, Mr. Emil Martisnek from AFRL/SNZ, and Dr. Jeffery Berrie from MRC for their sponsorship and advice throughout my research. Special recognition goes to Dr. Mark Scott from MRC whose knowledge in magnetism has been more than a great help with my work. Also, thanks goes to Andrew Bogle for instructing me on the stripline and its measurement technique.

Finally, the most important acknowledgment goes to my lovely wife Shana, without her I would not be the person I am today.

# TABLE OF CONTENTS

LIST OF TABLES .....	vi
LIST OF FIGURES .....	vii
CHAPTER 1 - Introduction .....	1
1.1 – Introduction.....	1
1.2 – Permittivity .....	1
1.3 – Permeability.....	3
1.4 - Overview .....	3
CHAPTER 2 – Dielectric and Magnetic Properties .....	6
2.1 - Permittivity .....	6
2.2 - Permeability.....	9
2.3 – Domains .....	14
2.4 - Magnetic Materials .....	16
CHAPTER 3 – Mixture and Measurement.....	18
3.1 - COD Composites.....	18
3.2 - Stripline Procedure .....	19
CHAPTER 4 – Mixing Formulations .....	22
4.1 - Maxwell Garnett Permittivity.....	22
4.2 - Clausius Mosotti Permittivity.....	27
4.3 – Bruggeman Permittivity.....	35
4.4 - Coherent Potential Permittivity .....	41
4.5 - Maxwell Garnett Permeability.....	47
4.6 – Bruggeman Permeability .....	50
4.7 - Coherent Potential Permeability.....	55
4.8 - Onsager Permeability .....	59
CHAPTER 5 - Applications.....	65
5.1 - Square Patch Antenna Bandwidth .....	65
CHAPTER 6 – Conclusions and Future Work .....	71
6.1 - Conclusion.....	71
6.2 - Future Work.....	73

# LIST OF TABLES

Table 1: Summary of major mixing formulas [22]..... 5

# LIST OF FIGURES

Figure 1: Description of dielectric mixture with spherical inclusions placed in an environment. $\epsilon_i$ is the permittivity of inclusions, $\epsilon_e$ is the permittivity of the environment. $\mu_i$ is the permeability of inclusions, $\mu_e$ is the permeability of the environment. ....	2
Figure 2.1.1: Description of polarization mechanisms [6]. ....	7
Figure 2.2.1: Model of a magnetic field due to an electron moving along its orbital around the nucleus. ....	9
Figure 2.2.2: Illustration of orbital angular momentum in the z-direction for a d-orbital. ....	11
Figure 2.3.1: Bloch wall transition for adjacent domains with anti-parallel magnetizations [25].....	15
Figure 2.4.1: (a) magnetic moments randomly aligned in absence of magnetic field, (b) magnetic moments exposed to applied magnetic field. ....	17
Figure 3.1.1: Types of composites for magnetic mixing [1].....	19
Figure 3.2.1: Description of stripline used in measurements [8].....	19
Figure 3.2.2: Description of three cascaded two port networks; region a, region b, and region s.....	20
Figure 4.1.1: Description of dielectric mixture with spherical inclusions placed in an environment. $\epsilon_i$ is the permittivity of inclusions, $\epsilon_e$ is the permittivity of the environment. ....	22
Figure 4.1.2: Plot of effective permittivity vs. changing volume fraction. $\epsilon_e = 3.5$ and $\epsilon_i = 16$ .....	24
Figure 4.1.3: Maxwell Garnett calculated permittivity graphed with measured permittivity of a sample with volume fraction $f=0.4$ . ....	26
Figure 4.1.4: Maxwell Garnett calculated permittivity graphed with measured permittivity of a sample with volume fraction $f=0.25$ . ....	26
Figure 4.1.5: Maxwell Garnett calculated permittivity graphed with measured permittivity of a sample with volume fraction $f=0.1$ . ....	27

Figure 4.2.1: Electric fields by a spherical inclusion. $\bar{E}$ is the applied field, and $\bar{P}$ is the field inside the particle. ....	28
Figure 4.2.2: Clausius Mosotti calculated permittivity graphed with measured permittivity of a sample with volume fraction $f=0.4$ . ....	31
Figure 4.2.3: Clausius Mosotti calculated permittivity graphed with measured permittivity of a sample with volume fraction $f=0.25$ . ....	31
Figure 4.2.4: Clausius Mosotti calculated permittivity graphed with measured permittivity of a sample with volume fraction $f=0.1$ . ....	32
Figure 4.2.5: Comparison of Clausius Mosotti to Maxwell Garnett and Experimental data for $f=0.4$ .....	33
Figure 4.2.6: Comparison of Clausius Mosotti to Maxwell Garnett and Experimental data for $f=0.25$ . ....	33
Figure 4.2.7: Comparison of Clausius Mosotti to Maxwell Garnett and Experimental data for $f=0.1$ . ....	34
Figure 4.3.1: Bruggeman calculated permittivity graphed with measured permittivity of a sample with volume fraction $f=0.4$ . ....	37
Figure 4.3.2: Bruggeman calculated permittivity graphed with measured permittivity of a sample with volume fraction $f=0.25$ . ....	37
Figure 4.3.3: Bruggeman calculated permittivity graphed with measured permittivity of a sample with volume fraction $f=0.1$ . ....	38
Figure 4.3.4: Maxwell Garnett, Bruggeman, and Experimental data graphed for comparison for $f=0.4$ . ....	39
Figure 4.3.5: Maxwell Garnett, Bruggeman, and Experimental data graphed for comparison for $f=0.25$ . ....	39
Figure 4.3.6: Maxwell Garnett, Bruggeman, and Experimental data graphed for comparison for $f=0.1$ . ....	40
Figure 4.4.1: Coherent Potential calculated permittivity graphed with measured permittivity of a sample with volume fraction $f=0.4$ . ....	43
Figure 4.4.2: Coherent Potential calculated permittivity graphed with measured permittivity of a sample with volume fraction $f=0.25$ . ....	44

Figure 4.4.3: Coherent Potential calculated permittivity graphed with measured permittivity of a sample with volume fraction $f=0.1$ .....	44
Figure 4.4.4: Maxwell Garnett, Bruggeman, Coherent Potential, and Experimental data graphed for comparison for $f=0.4$ .....	45
Figure 4.4.5: Maxwell Garnett, Bruggeman, Coherent Potential, and Experimental data graphed for comparison for $f=0.25$ .....	46
Figure 4.4.6: Maxwell Garnett, Bruggeman, Coherent Potential, and Experimental data graphed for comparison for $f=0.1$ .....	46
Figure 4.5.1: Maxwell Garnett calculated permeability graphed with measured permittivity of a sample with volume fraction $f=0.4$ .....	48
Figure 4.5.2: Maxwell Garnett calculated permeability graphed with measured permittivity of a sample with volume fraction $f=0.25$ .....	48
Figure 4.5.3: Maxwell Garnett calculated permeability graphed with measured permittivity of a sample with volume fraction $f=0.1$ .....	49
Figure 4.6.1: Bruggeman calculated permeability graphed with measured permeability of the sample with volume fraction $f=0.4$ .....	51
Figure 4.6.2: Bruggeman calculated permeability graphed with measured permeability of the sample with volume fraction $f=0.25$ .....	51
Figure 4.6.3: Bruggeman calculated permeability graphed with measured permeability of the sample with volume fraction $f=0.1$ .....	52
Figure 4.6.4: Maxwell Garnett, Bruggeman, and Experimental data graphed for comparison for $f=0.4$ .....	53
Figure 4.6.5: Maxwell Garnett, Bruggeman, and Experimental data graphed for comparison for $f=0.25$ .....	53
Figure 4.6.6: Maxwell Garnett, Bruggeman, and Experimental data graphed for comparison for $f=0.1$ .....	54
Figure 4.7.1: Coherent Potential calculated permeability graphed with measured permittivity of a sample with volume fraction $f=0.4$ .....	55
Figure 4.7.2: Coherent Potential calculated permeability graphed with measured permittivity of a sample with volume fraction $f=0.25$ .....	56

Figure 4.7.3: Coherent Potential calculated permeability graphed with measured permittivity of a sample with volume fraction $f=0.1$ .....	56
Figure 4.7.4: Maxwell Garnett, Bruggeman, Coherent Potential and Experimental data graphed for comparison when $f=0.4$ .....	57
Figure 4.7.5: Maxwell Garnett, Bruggeman, Coherent Potential and Experimental data graphed for comparison when $f=0.25$ .....	58
Figure 4.7.6: Maxwell Garnett, Bruggeman, Coherent Potential and Experimental data graphed for comparison when $f=0.1$ .....	58
Figure 5.1.1: Bandwidth for constant permittivity with permeability varying from 1 to 10.....	66
Figure 5.1.2: Bandwidth for constant permeability with permittivity varying from 1 to 10.....	67
Figure 5.1.3: Bandwidth plot for permittivity of 2.2 and permeability of 2.....	68
Figure 5.1.4: Bandwidth plot for permittivity of 5.1 and permeability of 1.5.....	69
Figure 5.1.5: Bandwidth plot for permittivity of 4.4 and permeability of 1.....	70
Figure 6.1.1: Comparison of volume percent to weight percent.....	72
Figure 6.2.1: Types of composites.....	73

# CHAPTER 1 - Introduction

## 1.1 – Introduction

Materials inherently have dielectric and magnetic properties which describe how they interact with electromagnetic energy. Knowing these properties allows for a wide range of uses for many materials. However, sometimes it is desirable to mix or combine different materials in order to achieve the desired parameters. When this happens, it becomes increasingly difficult to predict the values of the effective permeability ( $\mu_{eff}$ ) and effective permittivity ( $\epsilon_{eff}$ ). This has been the focus of research and study for over a hundred years. Dielectric mixture theory was developed as far back as 1891 when Maxwell tackled the problem of obtaining the electromagnetic characteristics of simple magnetic mixtures [22]. The method for obtaining the dielectric properties has been the bulk of the research over the years because most materials have an effective permeability equal to one, unless dealing specifically with magnetism. Also, the mathematics involved with solving for  $\epsilon_{eff}$  is significantly less difficult and its behavior is more easily predictable.

## 1.2 – Permittivity

Many classical approaches are available for determining the effective permittivity of a mixture. Table 1 shows many of these approaches; however the four reviewed in this thesis are Maxwell-Garnett, Clausius Mosotti, Bruggeman, and Coherent Potential [20]. The first two of these formulations, Maxwell Garnett and Clausius Mosotti, focus on the inclusions affecting the mixture by being dispersed throughout a background medium

while the latter two cases approach the effective permittivity as an equal contribution from the background as from the inclusions based on their respective volume fractions. These models involve small dielectric spherical particles dispersed in a background with a different permittivity. This is illustrated in figure 1.2.1.

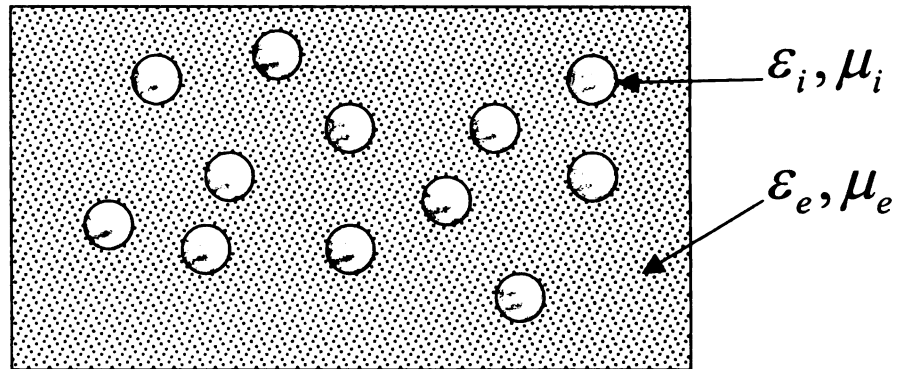


Figure 1: Description of dielectric mixture with spherical inclusions placed in an environment.  $\epsilon_i$  is the permittivity of inclusions,  $\epsilon_e$  is the permittivity of the environment.  $\mu_i$  is the permeability of inclusions,  $\mu_e$  is the permeability of the environment.

The ratio of inclusion volume to volume of the environment is called the volume fraction ( $f$ ). It will be shown how Maxwell-Garnett formulation, which looks at the effective permittivity as an averaged value, relying heavily on volume fraction as well as the permittivities of the inclusions and environment. Clausius Mosotti takes a different approach by replacing each inclusion with a dipole moment as a result of the polarizability of each spherical particle. These are two common and very basic mixing principles and will be derived then compared to measured data. Bruggeman theory is also analyzed for permittivity which looks at the effective permittivity as a result of the inclusions and environment equally as much. Another well-known formula which is relevant in the theoretical studies of wave propagation in random media is the so-called

Coherent Potential formula [20]. These latter two principles are also compared to the measured data. The basis from which these concepts arise is electrostatics. A static electric field can be defined simply as an electric field that does not change with time [4]. These assumptions can be made because the particle size is much smaller than a wavelength. The maximum diameter a particle can be in order to make this approximation is  $d_{\max}$  and is directly proportional to wavelength [11].

$$d_{\max} \cong \frac{\lambda}{2\pi} \quad (1.2.1)$$

### **1.3 – Permeability**

By the concept of duality, the electrostatic and magnetostatic problems are dual for any given geometry [12]. Therefore the permeability would seem to be found by the same methods as was done for permittivity simply by exchanging  $\mu$  for  $\epsilon$ . The permeability of the hexaferrite sample is compared to actual measured data using the classical mixing models: Maxwell Garnett, Bruggeman, and Coherent Potential. Also, an important mixing rule for effective permeability derived using Onsager's field relations is demonstrated for ferromagnetic materials [5, 19].

### **1.4 - Overview**

One application of predicting the values for  $\mu_{eff}$  and  $\epsilon_{eff}$  is to find various engineering design parameters such as the bandwidth of a square patch antenna with the mixed material as the substrate background [7]. The material chosen for use in this thesis is a

hexaferrite spherical inclusion dispersed in a non-magnetic background. A closer look at the geometry of this mixture can be seen in Figure 1.

In magnetism, hexaferrite is considered to be a ferrimagnetic material and was chosen because of its low conductivity,  $10^{-4}$  to 1 [18]. Another important characteristic is its ability to maintain magnetic non-trivial properties at higher frequencies as compared to ferromagnetic materials. Mixing becomes desirable when the properties of the material alone do not allow for the necessary interaction with EM fields. For example, ferromagnetic materials are often mixed in order to obtain a lower conductivity, yet retain its desirable magnetic behavior. Ferrimagnetic materials which are used in this thesis are mixed in order to obtain a relative permittivity that is lower, while retaining its magnetic properties. If permittivity is lowered enough to be the same as permeability then desirable matching characteristics are obtained in a square patch antenna or other devices. This is because the reflection coefficient of the material goes to zero when the permeability and permittivity are equal to each other. Also, the weight can be reduced if mixed with a less dense material which is a very desirable characteristic.

The format of this thesis is as follows: First, a background on dielectric and magnetic properties of materials is given, followed by a description of the measurement techniques used to find the actual permeability and permittivity of the material. Then a few classical methods are analyzed for permittivity, and later applied to permeability. Next will be a description of one application which is that of bandwidth for a patch antenna, and finally conclusions and suggested future work.

Description	Mixture Formula
Maxwell, 1891, spheres, 2-phase Maxwell Garnett formula [15]	$\varepsilon = \varepsilon_e + \frac{3V_i \varepsilon_e}{[(\varepsilon_i + 2\varepsilon_e)/(\varepsilon_i - \varepsilon_e)] - V_i}$
Rayleigh, 1892, spheres, 2-phase [14]	$\frac{\varepsilon - \varepsilon_e}{\varepsilon + 2\varepsilon_e} = V_i \left( \frac{\varepsilon_i - \varepsilon_e}{\varepsilon_i + 2\varepsilon_e} \right)$
Wiener, 1912, arbitrary shape, 2-phase; $u$ =form factor; $u = 2\varepsilon_e$ for spheres; $u = 2\varepsilon_i$ for disks; $u = 1/2(\varepsilon_i - 3\varepsilon_e)$ for needles [23]	$\frac{\varepsilon - \varepsilon_e}{\varepsilon + u} = V_i \left( \frac{\varepsilon_i - \varepsilon_e}{\varepsilon_i + u} \right)$
Bruggeman, 1935 spheres, 2-phase [3]	$\frac{\varepsilon_i - \varepsilon}{\varepsilon_i - \varepsilon_e} = (1 - V_i) \left( \frac{\varepsilon}{\varepsilon_e} \right)^{1/3}$
Böttcher, 1945, spheres, 2-phase [2]	$\frac{\varepsilon - \varepsilon_e}{3\varepsilon} = V_i \left( \frac{\varepsilon_i - \varepsilon_e}{\varepsilon_i + 2\varepsilon} \right)$
Polder, van Santen, 1946 ellipsoids, multiphase [17]	$\varepsilon - \varepsilon_e = \sum_{i=1}^N V_i (\varepsilon_i - \varepsilon_e) \frac{E_{\text{int}}}{E_{\text{ave}}}$ where $\frac{E_{\text{int}}}{E_{\text{ave}}} = \frac{1}{3} \sum_{j=1}^3 \left[ 1 + N_j \left( \frac{\varepsilon_j - \varepsilon}{\varepsilon} - 1 \right) \right]^{-1}$
Looyenga, 1965 spheres, 2-phase [13]	$\varepsilon^{1/3} = V_i \varepsilon_i^{1/3} + (1 - V_i) \varepsilon_e^{1/3}$
Sihvola, Kong, 1988 ellipsoids, random orientation [11]	$\varepsilon = \varepsilon_h + \sum_{i=1}^3 \frac{V(\varepsilon_i - \varepsilon_h) \varepsilon_a + N_i (\varepsilon - \varepsilon_h)}{3[\varepsilon_a + N_i (\varepsilon_i - \varepsilon_h)]}$ where $\varepsilon_a = \varepsilon_h + a(\varepsilon - \varepsilon_h)$ OR $\varepsilon = \varepsilon_h + \frac{\sum_{i=1}^3 \frac{V \varepsilon_a (\varepsilon_i - \varepsilon_h)}{2[\varepsilon_a + N_i (\varepsilon_i - \varepsilon_h)]}}{1 - \sum_{i=1}^3 \frac{V N_i (\varepsilon_i - \varepsilon_h)}{3[\varepsilon_a + N_i (\varepsilon_i - \varepsilon_h)]}}$

Table 1: Summary of major mixing formulas [22].

## CHAPTER 2 – Dielectric and Magnetic Properties

### 2.1 - Permittivity

In a microscopic sense, the electronic properties of matter depend on how tightly the electrons are bound [6]. Materials with loosely bound electrons are called conductors. When a conductor is placed in an electric field the electrons move in the opposite direction with respect to the applied field. However, materials with tightly bound electrons are called dielectrics. A dielectric material is a nonconductor of electric charge in which an applied electric field causes a displacement of charge but not a flow of charge [9]. This displacement involves moving the positive charges in the direction of the applied field, and the negative charges in the direction opposing the field which results in an electric dipole with its moment in the direction of the applied field. The collection of such dipoles is represented by an electric polarization ( $\bar{P}$ ).

The phenomenon of electronic polarization is caused by the displacement of the charge center of the electron cloud with respect to the nucleus [20]. Again, at the microscopic level, the polarization can be described with three mechanisms: electronic, atomic, and orientational polarization [6, 20]. This is illustrated in Figure 2.1.1. Atomic, or ionic, polarization occurs in materials where the molecules are formed by atoms which are bound together with ionic bonds. The dipole formation occurs when an electric field distorts the molecular orbit so that a net negative and positive charge center is created [6].

Mechanism	No applied field	Applied field
<b>Orientational Polarization</b>		
<b>Atomic Polarization</b>		
<b>Electronic Polarization</b>		

Figure 2.1.1: Description of polarization mechanisms [6].

Orientational polarization occurs in polar materials that already have dipoles even in the absence of an applied field. However, those dipoles are aligned randomly and have zero net polarization until an electric field is applied causing the already existing dipoles to align with the field. The electronic polarization vector  $\bar{P}$  can be described as the sum of dipole moments per unit volume, and can be represented by equation (2.1.1) where the strength of a dipole moment  $p$  can be represented by equation (2.1.2).

$$\bar{P} = N\bar{p} \quad (2.1.1)$$

$$\bar{p} = Qd\hat{u} \quad (2.1.2)$$

$N$  is the number density of dipoles,  $Q$  is the magnitude of a charge,  $d$  is the separation between the positive and negative charges, and  $\hat{u}$  is the alignment of the dipole from the negative to positive charge.

These dipole effects divide dielectric materials into four groups based on their polarization mechanisms: nonpolar, polar, electret, and ferroelectric [6]. Nonpolar materials do not have any dipole moments in the absence of an applied field, but does have a net polarization when a field is applied. Polar materials, on the other hand, do have dipole moments when there is no impressed field but are aligned randomly and cancel out so there is no net polarization. However, polar materials do form a net polarization in an applied field. Electret materials do possess a net polarization in the absence of an electric field, and ferroelectric materials have a nonlinear reaction to an applied field, and can have a remnant polarization when the applied field is removed [6].

Electric flux density  $\bar{D}$  can be represented by the electric flux density in a vacuum  $\bar{D}_0$  plus the polarization  $\bar{P}$  of the medium. This is shown in equation (2.1.3).

$$\bar{D} = \bar{D}_0 + \bar{P} \quad (2.1.3)$$

Where  $\bar{D}_0$  and  $\bar{P}$  can be represented

$$\bar{D}_0 = \epsilon_0 \bar{E} \quad (2.1.4)$$

$$\bar{P} = \epsilon_0 \chi_e \bar{E} \quad (2.1.5)$$

where  $\epsilon_0$  is the permittivity of free space,  $\bar{E}$  is the applied electric field,  $\chi_e = \epsilon_r - 1$  is the electric susceptibility and  $\epsilon_r$  is the relative permittivity of the medium. The permittivity is a bulk property of a dielectric material and can be used to describe its reaction to an applied electric field. The relative permittivity of a mixture is one of the desired characteristics that will be discussed in this thesis.

## 2.2 - Permeability

Unlike the dielectric properties of matter previously described, the magnetic behavior needs to be analyzed more rigorously in order to be accurate, making it much more challenging. The magnetic effects can be the result of one or all of the following three things: net nuclear spin, asymmetric electron orbital, and net electron spin [6]. Generally the nuclear spin contribution is much less than the contributions from the electron orbital and spin. According to quantum theory, electrons can have a spin-up or a spin-down state and an orbital is allowed to have only one of each spin state. A net magnetic field will be produced if an orbital has only one electron due to its spin. A magnetic field will also be produced by the movement of that electron along its orbital. These are the two major contributions to the magnetic behavior due to its electrons.

The magnetic field due to the electron traveling along its orbital can be modeled as a magnetic moment. A current is produced by the moving charge, and since the current is traveling in a loop a magnetic field is produced according to the right hand rule. This is illustrated in Figure 2.2.1.

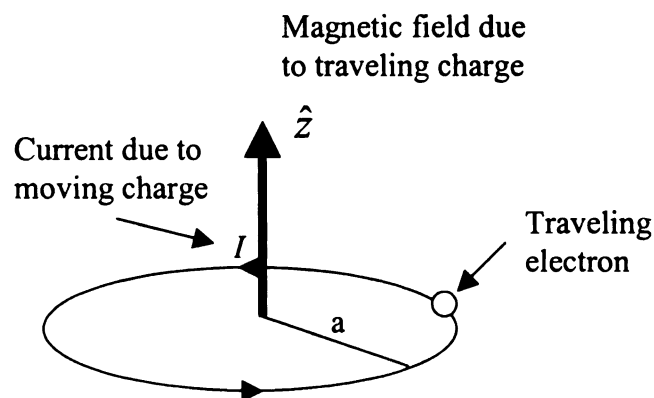


Figure 2.2.1: Model of a magnetic field due to an electron moving along its orbital around the nucleus.

This field can be represented as the magnetic dipole moment due to the circling charge.

$$\bar{m} = \hat{z}I\pi a^2 \quad (2.2.1)$$

Where  $\bar{m}$  is the magnetic dipole moment,  $I$  is the current due to the electron and is multiplied by the surface area of the orbital [18]. This model can be taken into further consideration because these electrons can only have specific energy states and the orbitals have specific positions. The principal quantum number  $n$  is the value that determines the energy of a particular shell or orbit [16]. This number gives us the orbital angular momentum quantum number  $l$ .

$$l = 0, 1, 2, \dots, (n - 1) \quad (2.2.2)$$

$$M = \hbar\sqrt{l(l+1)} \quad (2.2.3)$$

$M$  is the total angular momentum of an electron due to its orbital motion, and  $\hbar$  is Planck's constant. The magnetic quantum number  $m_l$  determines the component of the orbital momentum along the direction of the applied magnetic field [16]. Therefore the angular momentum in the z-direction can be determined by equation (2.2.4). This is illustrated in Figure 2.2.2 for a d-orbital ( $l=2$ ).

$$M_z = m_l\hbar \quad (2.2.4)$$

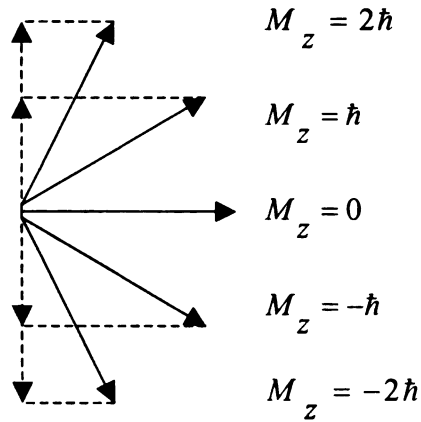


Figure 2.2.2: Illustration of orbital angular momentum in the z-direction for a d-orbital.

Next, the intrinsic angular momentum is caused by the electron spinning about an internal axis. The spin quantum number ( $m_s$ ) determines the component of the spin ( $s$ ) along the direction of the applied field [16]. Unlike the orbital angular momentum, this number is restricted to  $\pm 1/2$ . Thus the contribution of the spin angular momentum in the  $\pm z$ -direction is restricted to  $\pm \hbar/2$ .

$$S_z = m_s \hbar \quad (2.2.5)$$

By quantum mechanical theory the total angular momentum  $\bar{J}\hbar$  of an atom containing a number of electrons is equal to the sum of the total orbital angular momentum  $\bar{M}\hbar$  and the total spin angular momentum  $\bar{S}\hbar$  [21].

$$\bar{J} = \bar{M} + \bar{S} \quad (2.2.6)$$

The orbital and spin magnetic moments that result from these values is seen in equations (2.2.7) and (2.2.8).

$$m_L = -\sqrt{M(M+1)} \left( \frac{\mu_0 e \hbar}{2m} \right) \quad (2.2.7)$$

$$m_S = -\sqrt{S(S+1)} \left( \frac{\mu_0 e \hbar}{2m} \right) \quad (2.2.8)$$

Where  $e$  is the charge of an electron and  $m$  is the mass of an electron. Since the charge of an electron is negative, the magnetic moments are directed opposite to the vector sums of their angular momentum [21]. The effective magnetic moment  $m_J$  of the atom is directed along the same direction as  $\bar{J}$  and is shown in equation (2.2.9).

$$m_J = -g \sqrt{J(J+1)} \left( \frac{\mu_0 e \hbar}{2m} \right) \quad (2.2.9)$$

$$g = 1 + \frac{J(J+1) + S(S+1) - M(M-1)}{2J(J+1)} \quad (2.2.10)$$

$g$  is known as the Lande  $g$ -factor and it determines the splitting of the energy levels in the presence of a weak external magnetic field [21]. When an atom with a nonzero net magnetic moment is exposed to an externally applied magnetic field its total angular momentum precesses, moves with a gyrating fashion, about the magnetic field lines. This happens because the electrons are fixed to their orbitals, therefore  $\bar{J}$  precesses about the field lines and not the electron itself. When there is more than one atom present, the predictions become more complicated because of coupling between the different atoms [6]. The orbital contributions to the net magnetic moment tend to cancel due to their alignment in the crystalline phase of the transition metals [21]. The coupling that occurs

between adjacent atoms is due to their spins and can be represented by exchange energy  $W_{ex}$ .

$$W_{ex} = -2J_e S_i \cdot S_j \quad (2.2.11)$$

$$J_e = \frac{3kT_c}{2ZS(S+1)} \quad (2.2.12)$$

In equation (2.2.12)  $k$  is Boltzmann's constant,  $T_c$  is the Curie temperature, and  $Z$  is the number of nearest neighbors.  $S_i$  and  $S_j$  are the total spin angular momentums of the atoms located at  $i$  and  $j$  respectively.  $J_e$  is known as the exchange integral which expresses the difference in Coulomb interaction energy of the system when the spins are parallel or anti-parallel [21]. For atoms with spins aligned parallel to each other,  $J_e$  is positive and the result is ferromagnetism and there is a net magnetic moment due to those atoms. However, if the spins are anti-parallel  $J_e$  is negative and the result is anti-ferromagnetism with a net magnetic moment of zero due to those atoms.

When looking at a magnetic material in a macroscopic sense, there exists a magnetic polarization vector similar to the electric polarization vector discussed in the dielectric material section. The magnetic flux density  $\bar{B}$  that results from an applied field  $\bar{H}$  is the sum of the flux density in a vacuum  $\bar{B}_0$  and the magnetic polarization vector of the material  $\bar{M}$ , commonly referred to as magnetization.

$$\bar{B} = \bar{B}_0 + \bar{M} \quad (2.2.13)$$

where

$$\bar{B}_0 = \mu_0 \bar{H} \quad (2.2.14)$$

$$\bar{M} = \mu_0 \chi_m \bar{H} \quad (2.2.15)$$

$\bar{H}$  is the static applied field,  $\mu_0$  is the permeability of free space,  $\chi_m = \mu_r - 1$  is the susceptibility, and  $\mu_r$  is the bulk relative permeability of the material. Equation (2.2.13) can now be written in terms of the static applied field and the permeability.

$$\bar{B} = \mu_0 \mu_r \bar{H} = \mu \bar{H} \quad (2.2.16)$$

Permeability is a very important quantity in electromagnetics and is part of the focus of this thesis.

### **2.3 – Domains**

In section 2.2, the magnetic moment was described for a single atom. When adjacent atoms have parallel moments they form a domain within the material. The domain will have a net magnetization in the direction of the aligned moments within it. In an unmagnetized material the domains randomly align yielding a net magnetization of zero. How these domains react to an externally applied field determines its type of magnetic material. The transition layer between adjacent domains magnetized in different directions is called a Bloch wall. The thickness of this wall is found from the exchange energy, which tends to increase its thickness, and the anisotropy energy, which tends to decrease its thickness [21]. For example the wall thickness for iron with domains whose

magnetization is aligned anti-parallel is about  $10^{-7}$  meters [21]. Figure 2.3.1 illustrates this transition region.

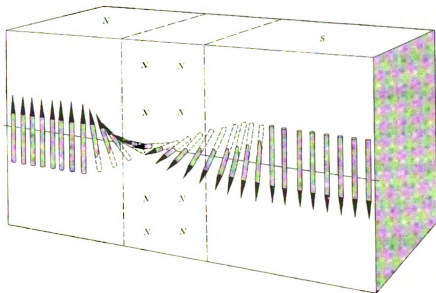


Figure 2.3.1: Bloch wall transition for adjacent domains with anti-parallel magnetizations [25].

The mixture discussed in this thesis is assumed to have magnetic inclusions that are small enough that each particle is one single domain. When trying to find the effective permittivity and permeability of a mixture it is easier if the particles each represent only one net magnetization, whereas a multiple domain particle would have different magnetization directions within itself. The particles also need to be far enough away from adjacent particles in order to not interact with one another which can change the ability to be single domain. When this happens the material no longer exhibits the characteristics that were desired by a mixture of single domain inclusions.

## **2.4 - Magnetic Materials**

The sum of all magnetic moments in a volume is the magnetic polarization vector  $\overline{M}$ . This is also referred to as the saturation magnetization when all the magnetic dipoles in a volume are aligned along the applied magnetic field [6]. Depending on whether the sum of moments adds to or subtracts from an applied field, magnetic materials can be split into two categories. The first involves materials with relative permeabilities less than one, and whose magnetization vector acts against an applied field. This type of material is called a diamagnetic material. In the absence of an applied field, the orbital and spin moments cancel, and there is no net magnetic moment on each atom [18]. The second category involves those materials whose net moments align with an applied field. This type of material is called a paramagnetic material, and in the absence of an external field the spin moments are greater than the orbital moments leaving individual atoms with a net permanent magnetic moment. A common example of a paramagnetic material is that which is found in kitchen magnets. In either case, the density of magnetic moments  $\overline{M}$  is zero in the absence of an applied field [18]. In the second category, there are three sub-categories; ferromagnetic, anti-ferromagnetic, and ferrimagnetic materials.

Ferromagnetic materials, such as nickel and iron, have all their magnetic moments aligned and parallel to each other. Due to this alignment, ferromagnetic materials have a very high polarizability, otherwise known as magnetizability in terms of magnetism, and add to an applied field easily [20]. Regions where these aligned moments create a nonzero magnetization  $\overline{M}$  in the absence of an external field are called magnetic domains.

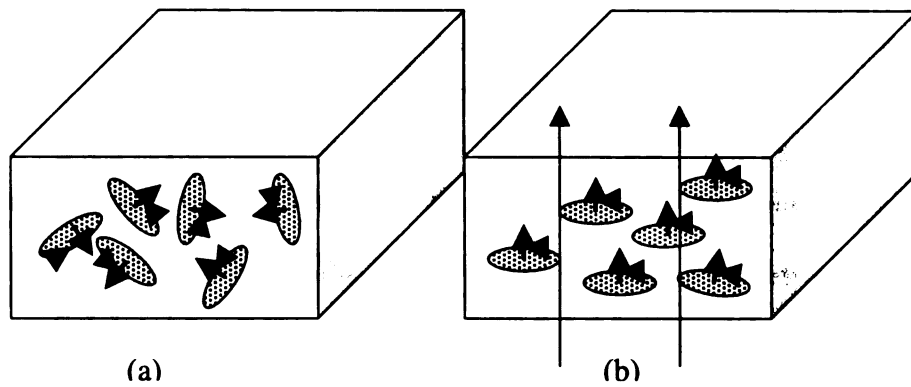


Figure 2.4.1: (a) magnetic moments randomly aligned in absence of magnetic field, (b) magnetic moments exposed to applied magnetic field.

In the macroscopic sense, these domains all orient in a way that the net magnetization is zero. Anti-ferromagnetic materials have magnetic moments which are aligned anti-parallel to each other canceling out any net magnetization. Because of this orientation the polarizability of anti-ferromagnetic materials is very low. Finally, ferrimagnetic materials have moments that also align anti-parallel to each other but they are not equal in magnitude resulting in a net magnetic field.

Ferrites are the material focused on in this thesis. Ferrites are considered a very useful group of ferrimagnetic materials. Developed in the 1940's by researchers at the Phillip Laboratories as low-loss magnetic media for supporting electromagnetic waves, ferrites have very low conductivity, very high relative permeability and relative permittivities in the range 10-15 [18]. The ability to maintain magnetic characteristics at higher frequencies is another benefit of ferrimagnetic materials. Also the saturation magnetization tends to be much higher than that of ferromagnetic materials.

## CHAPTER 3 – Mixture and Measurement

### 3.1 - C0D Composites

C0D composites are mixtures with magnetic inclusions, often spheroids and ellipsoids, embedded in a nonmagnetic medium [1]. The volume fraction ( $f$ ) of this material is the volume of the inclusions to the volume of the background and varies between 0 and 1. For example, when  $f=0.25$  then 25% of the total volume is the inclusions while 75% is the surrounding matrix. In this thesis, one type of material has spherical particles with a radius of approximately 2 microns and has been mixed with volume fractions of 0.1, 0.25, and 0.4. According to Sihvola and Kong [11], the maximum diameter of the spherical inclusions allowed in order to apply the rules of electrostatics and magnetostatics is given by equation 3.1.1.

$$d_{\max} \cong \frac{\lambda}{2\pi} \quad (3.1.1)$$

Here,  $\lambda$  is the wavelength of the incident field. This is a necessary assumption for application of the mixing principles. There has been a significant amount of work dedicated to determining the effective permeability and effective permittivity of such a mixture. Some of the classical methods will be looked at in this paper such as: Maxwell Garnett, Clausius Mosotti, etc. Figure 3.1.1 shows the C0D composite as well as C1D and C2D which represent respectively magnetic wires and magnetic thin films embedded in the background. The C1D and C2D composites will be discussed later in the section on future work.

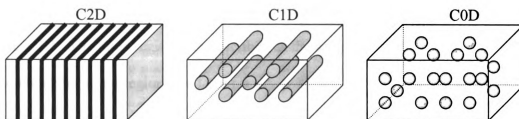


Figure 3.1.1: Types of composites for magnetic mixing [1].

### 3.2 - Stripline Procedure

The testing procedure for extraction of permeability and permittivity was done using a stripline waveguide and a network analyzer which is used to measure the S-parameters. Using the measured S-parameters and a root search program written in Matlab, we are able to obtain the complex permeability and permittivity of the sample over a wide bandwidth if necessary. Figure 3.2.1 shows the setup for the stripline waveguide and placement of the sample material. The tuning wedges are grounded, conducting, triangular structures which are used to maintain a nearly uniform width-to-height ratio.

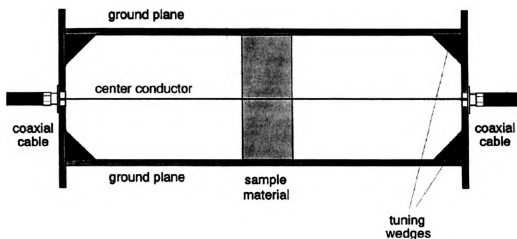


Figure 3.2.1: Description of stripline used in measurements [8].

The stripline is then split into three cascaded two port networks. This is illustrated in figure 3.2.2. The three regions are described as the sample region (  $s$  ) and the surrounding air filled regions (  $a$  ) and (  $b$  ).

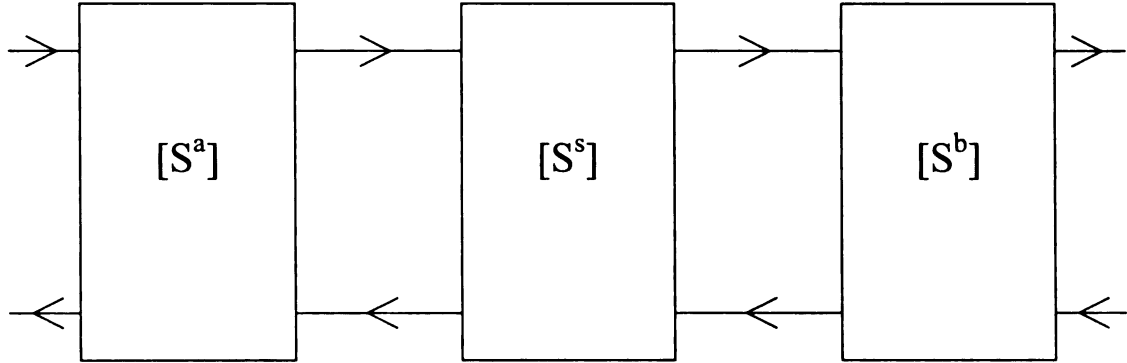


Figure 3.2.2: Description of three cascaded two port networks; region a, region b, and region s.

By equating the measured S-parameters with the following expressions, the interfacial reflection coefficient (  $\Gamma$  ) and the propagation factor (  $\beta$  ) is found.

$$S^s_{11} = \frac{\Gamma(1 - z^2)}{1 - (\Gamma z)^2} \quad (3.2.1)$$

$$S^s_{21} = \frac{z(1 - \Gamma^2)}{1 - (\Gamma z)^2} \quad (3.2.2)$$

$$z = e^{-j\beta l_s} \quad (3.2.3)$$

Where  $l_s$  is the thickness of the sample [8].

$$\beta = k = \frac{\omega}{c} \sqrt{\epsilon_r \mu_r} \quad (3.2.4)$$

Now using the values for  $\beta$  and  $\Gamma$  the relative permittivity and permeability can be determined using equations (3.2.5) and (3.2.6) respectively.

$$\epsilon_r = \frac{\beta}{k_0} \left( \frac{1-\Gamma}{1+\Gamma} \right) \quad (3.2.5)$$

$$\mu_r = \frac{\beta}{k_0} \left( \frac{1+\Gamma}{1-\Gamma} \right) \quad (3.2.6)$$

These equations are an example of how the complex relative permittivity and permeability of a sample placed in a waveguide can be determined. However, the stripline does not allow for measurements directly near the sample. Therefore, the  $S_{11}^s$  and  $S_{21}^s$  must be extracted from the S-parameters measured at the ends and the structure. This can be accomplished using a de-embedding technique. For more information on this technique, see Infante [8].

The stripline is very useful because it supports a transverse electromagnetic (TEM) wave, which has a zero frequency cutoff allowing for very low frequency measurements. Also, when the stripline is designed properly, the TEM wave will allow for a large bandwidth of 100 MHz up to 18 GHz [8]. The characteristic impedance of the structure is determined directly from its height and width, which allows for ease in the transition from the stripline to the coaxial cable.

## CHAPTER 4 – Mixing Formulations

### 4.1 – Maxwell-Garnett Permittivity

One of the more classical approaches to finding the permittivity of a mixture is the Maxwell-Garnett formula. This relation looks at a mixture of dielectric materials from a macroscopic viewpoint using volume-averaged fields. Consider Figure 4.1.1 in which spherical inclusions are randomly dispersed throughout a medium, called the environment or matrix.

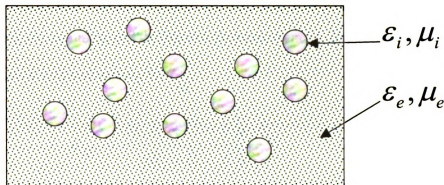


Figure 4.1.1: Description of dielectric mixture with spherical inclusions placed in an environment.  $\epsilon_i$  is the permittivity of inclusions,  $\epsilon_e$  is the permittivity of the environment.

The spherical particles are allowed to be randomly positioned, where  $f$  is the volume fraction of inclusions to environment. Therefore,  $1 - f$  is the volume fraction of the environment to the inclusions. Relating the macroscopic values of the electric flux density to electric field quantity gives the following:

$$\langle \bar{D} \rangle = \epsilon_{\text{eff}} \langle \bar{E} \rangle \quad (4.1.1)$$

$$\langle \bar{D} \rangle = \frac{1}{V} \int_V \bar{D} dV \quad (4.1.1a)$$

where  $\varepsilon_{eff}$  is the permittivity of the entire mixture and the symbol  $\langle \rangle$  denotes the volume average represented by equation (4.1.1a). Defining the macroscopic fields in terms of their volume fractions gives:

$$\langle \bar{D} \rangle = f\varepsilon_i E_i + (1-f)\varepsilon_e E_e \quad (4.1.2)$$

$$\langle \bar{E} \rangle = fE_i + (1-f)E_e \quad (4.1.3)$$

Where  $E_i$  is the magnitude of the field within the inclusion and  $E_e$  is the magnitude of the field surrounding the inclusion and throughout the environment. Inserting (4.1.2) and (4.1.3) into equation (4.1.1) and solving for  $\varepsilon_{eff}$ :

$$\varepsilon_{eff} = \frac{f\varepsilon_i E_i + (1-f)\varepsilon_e E_e}{fE_i + (1-f)E_e} \quad (4.1.4)$$

For an inclusion that is much smaller than a wavelength allowing for use of the electrostatic field solution and Rayleigh scattering by a spherical object [10],  $E_i$  and  $E_e$  can be replaced by the ratio  $E_e / E_i$ .

$$\frac{E_e}{E_i} = \frac{3\varepsilon_e}{\varepsilon_i + 2\varepsilon_e} \quad (4.1.5)$$

Formally dividing (4.1.4) by  $E_i$  and utilizing (4.1.5) yields the Maxwell Garnett mixing formula.

$$\epsilon_{eff} = \frac{f\epsilon_i + (1-f)\epsilon_e(3\epsilon_e/(\epsilon_i + 2\epsilon_e))}{f + (1-f)(3\epsilon_e/(\epsilon_i + 2\epsilon_e))} \quad (4.1.6)$$

Equation (4.1.6) can be rewritten in the more commonly seen form [20]:

$$\epsilon_{eff} = \epsilon_e + 3f\epsilon_e \frac{(\epsilon_i - \epsilon_e)}{\epsilon_i + 2\epsilon_e - f(\epsilon_i - \epsilon_e)} \quad (4.1.7)$$

This equation is considered to have a solid foundation in quasi-static cases where the size of the inclusions is much smaller than wavelength. Looking at a plot of relative permittivity found using equation (4.1.7) vs. the volume fraction one can look at the two extreme cases for a mixture purely made of inclusion and a mixture with no inclusions.

This is seen in Figure 4.1.2.

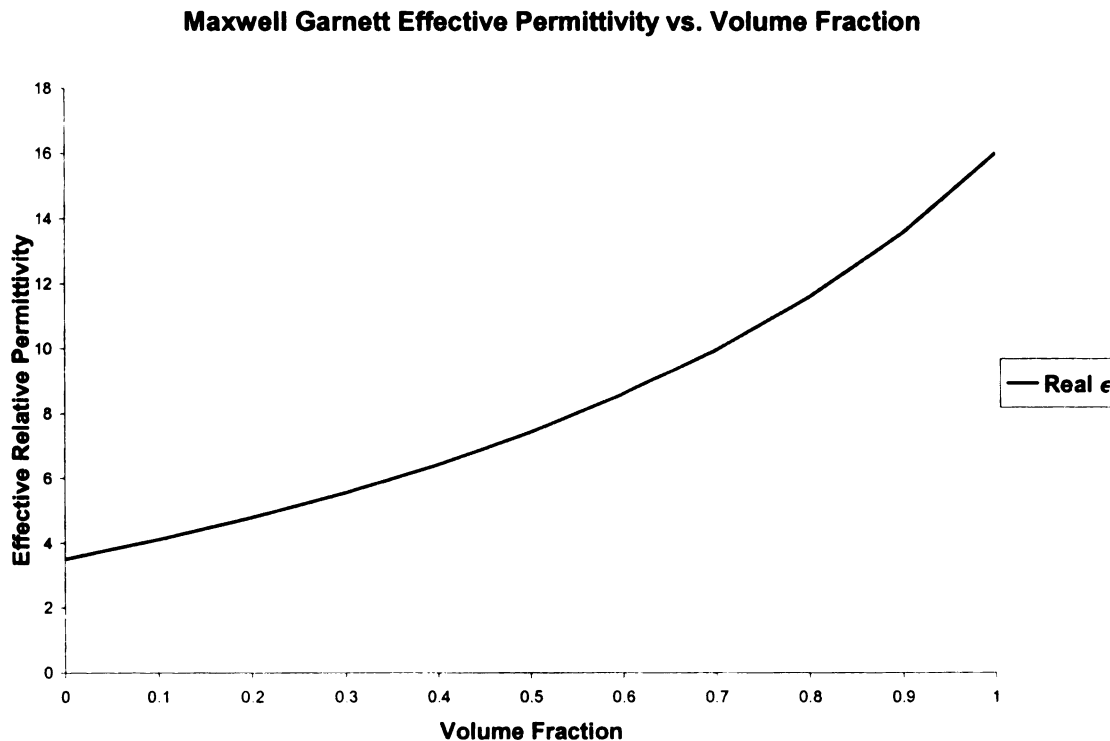


Figure 4.1.2: Plot of effective permittivity vs. changing volume fraction.  $\epsilon_e = 3.5$  and  $\epsilon_i = 16$ .

For a volume fraction of 0, corresponding to no inclusions, the equation reduces to  $\epsilon_{eff} = \epsilon_e$  which is just the permittivity of the environment alone. Also, for a volume fraction of 1, equation (4.1.7) becomes  $\epsilon_{eff} = \epsilon_i$  which is the permittivity of the inclusions. However, the latter case is not physically realizable because of the spherical shape of the inclusions it would be too difficult to get a volume fraction of 1 since there is always some interstitial volume. But this does show that the Maxwell Garnett formula should be accurate at least in the regions closer to the extreme cases.

Equation (4.1.7) has been graphed over a frequency range of 2 GHz to 12 GHz for three different volume fractions; 0.1, 0.25, and 0.4. The inclusions are hexaferrite spherical particles of permittivity 16 with a radius of  $1.91 \mu\text{m}$  dispersed in a background with a relative permittivity of 3.5. Although the calculated effective permittivity is independent of frequency it is easier to compare it to the measured data if it is plotted as constant over this range. Measured data is taken from our strip-line measurements. A detailed description of this measurement technique can be seen in section 3.2. Figures 4.1.3, 4.1.4 and 4.1.5 show these comparisons with volume fractions 0.4, 0.25, and 0.1 respectively.

### Maxwell Garnett Permittivity [ f=0.4 ]

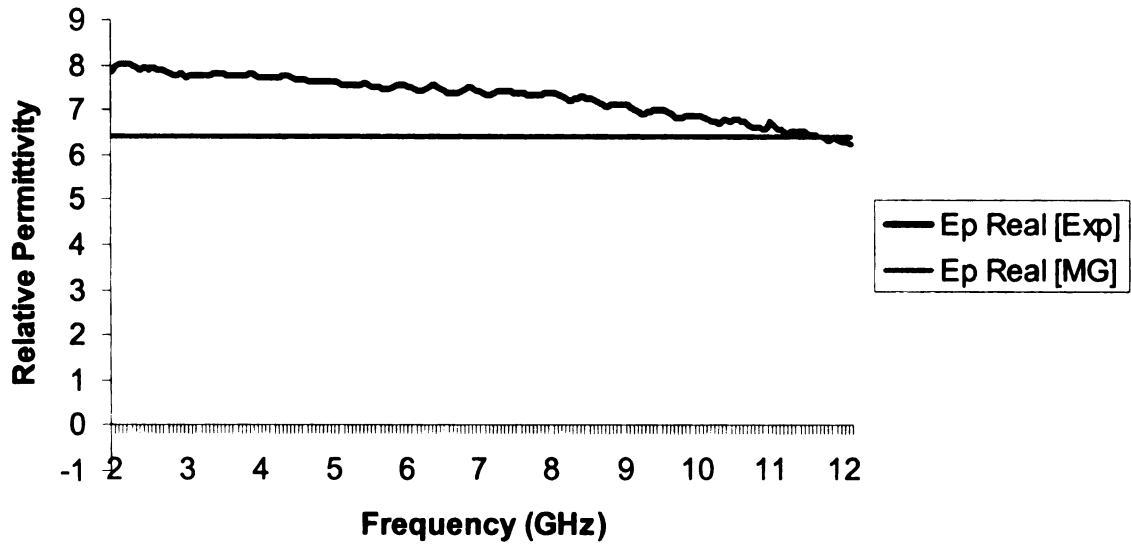


Figure 4.1.3: Maxwell Garnett calculated permittivity graphed with measured permittivity of a sample with volume fraction  $f=0.4$ .

### Maxwell Garnett Permittivity [ f=0.25 ]

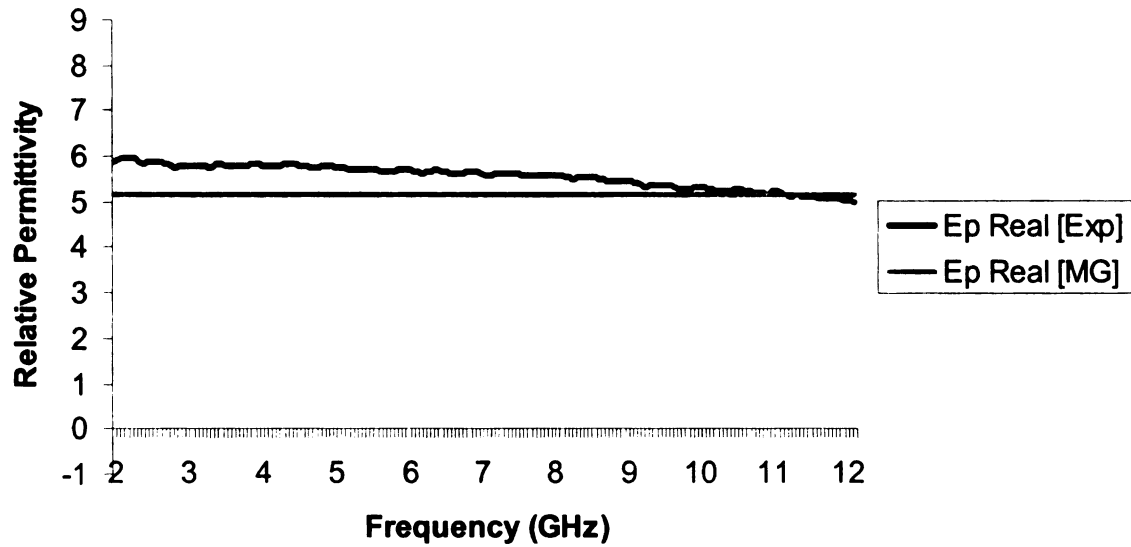


Figure 4.1.4: Maxwell Garnett calculated permittivity graphed with measured permittivity of a sample with volume fraction  $f=0.25$ .

## Maxwell Garnett Permittivity [ $f=0.1$ ]

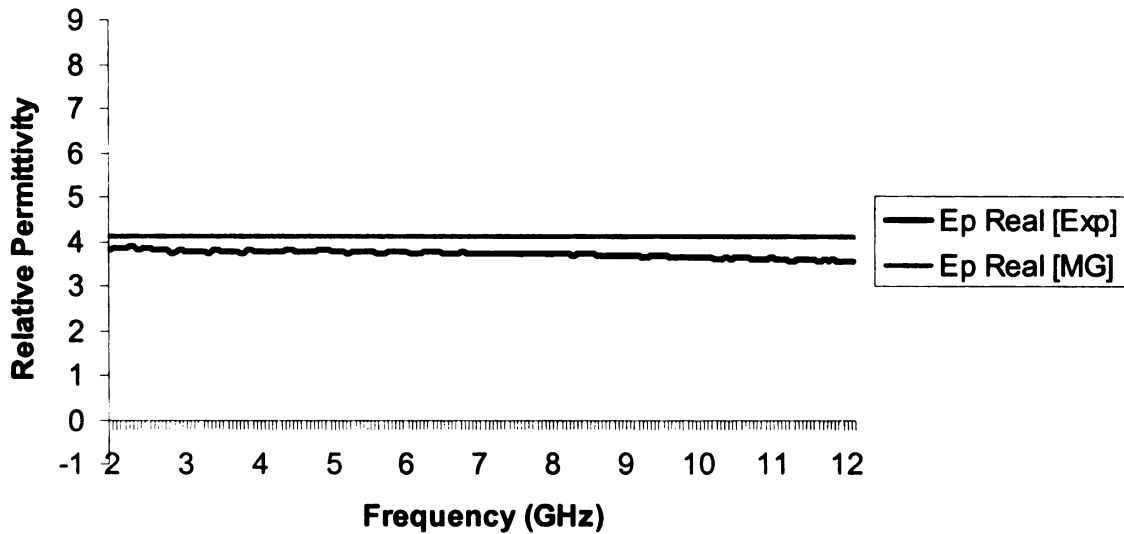


Figure 4.1.5: Maxwell Garnett calculated permittivity graphed with measured permittivity of a sample with volume fraction  $f=0.1$ .

These figures reveal that as volume fraction is reduced, the accuracy of Maxwell Garnett formulation becomes more accurate. This occurs because equation (4.1.7) does not take into consideration the effect of particle-particle interaction. As the volume fraction becomes smaller, the separation between adjacent inclusions is increased allowing for less, if any, interaction.

### 4.2 - Clausius Mosotti Permittivity

The Clausius Mosotti relation involves polarizability of the individual spherical inclusions. This polarization is averaged by replacing the scatterers with dipole moments [20].

The dipole moment  $\bar{p}$  of a particle can be defined by:

$$\bar{p} = \alpha \bar{E}' \quad ++(4.2.1)$$

where  $\alpha$  is the polarizability, and  $\bar{E}'$  is the local electric field.  $\bar{E}'$  can be represented by the *Mosotti* field [18].

$$\bar{E}' = \bar{E} + \frac{\bar{P}}{3\epsilon_0} \quad (4.2.2)$$

Where  $\bar{E}$  is the applied electric field,  $\bar{P}$  represents the macroscopic dipole moment density, also called the Electric Polarization vector, and  $\bar{P}/3\epsilon_0$  is the field resulting from the polarized molecules and is found outside the particle often called the “Lorentz field”.

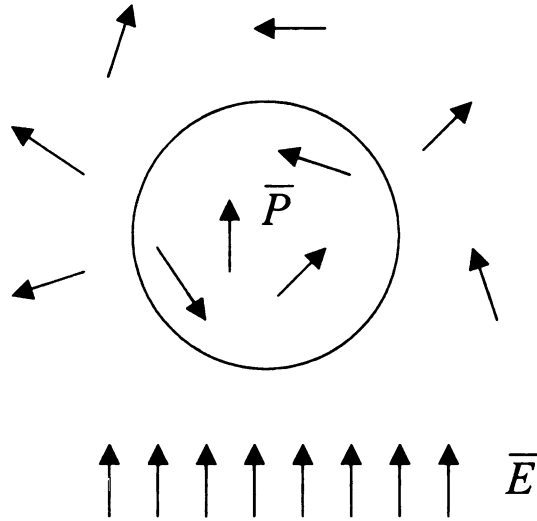


Figure 4.2.1: Electric fields by a spherical inclusion.  $\bar{E}$  is the applied field, and  $\bar{P}$  is the field inside the particle.

Using equation (4.2.2), the macroscopic dipole moment density  $\bar{P}$  can be found by:

$$\bar{P} = N\alpha \bar{E}' = N\alpha \left( \bar{E} + \frac{\bar{P}}{3\epsilon_0} \right) \quad (4.2.3)$$

where  $N$  is the number density of dipoles. Solving for  $\bar{P}$

$$\bar{P} = \left( \frac{3\epsilon_0 N\alpha}{3\epsilon_0 - N\alpha} \right) \bar{E} \quad (4.2.4)$$

This is the macroscopic dipole moment density found due to the applied field which is propagating in free space and can be represented  $\bar{P} = \chi_e \epsilon_0 \bar{E}$ .

$$\chi_e = \frac{3N\alpha}{3\epsilon_0 - N\alpha} \quad (4.2.5)$$

This is the susceptibility and can be represented  $\chi_e = \epsilon_r - 1$ . Using the susceptibility to solve for permittivity

$$\epsilon = \epsilon_0 \epsilon_r = \epsilon_0 \frac{3 + 2N\alpha / \epsilon_0}{3 - N\alpha / \epsilon_0} \quad (4.2.6)$$

and rearranging to solve for polarizability

$$\alpha = \frac{3\epsilon_0(\epsilon_r - 1)}{N(\epsilon_r + 2)} \quad (4.2.7)$$

gives the *Clausius Mosotti formula* for polarizability [18]. Equations (4.2.6) and (4.2.7) can be manipulated to describe a spherical inclusion surrounded by a dielectric medium.

By replacing  $\epsilon_0$  with  $\epsilon_e$  for the relative permittivity of the environment in equation

(4.2.6) and writing (4.2.7) in terms of a dielectric sphere

$$\epsilon_{eff} = \epsilon_e \frac{3 + 2N\alpha / \epsilon_e}{3 - N\alpha / \epsilon_e} \quad (4.2.8)$$

Remembering that  $\bar{p} = \alpha \bar{E}$ ,  $\bar{p} = V \bar{P}$  and using the static field solution for a dielectric sphere immersed in a field (4.2.9)

$$E_i = \frac{3\epsilon_e}{\epsilon_i + 2\epsilon_e} E_e \quad (4.2.9)$$

the polarizability  $\alpha$  can be found to be

$$\alpha = 3\epsilon_e V \frac{\epsilon_i - \epsilon_e}{\epsilon_i + 2\epsilon_e} \quad (4.2.10)$$

$V$  is the volume of the spherical particles. Equations (4.2.8) and (4.2.10) will give the effective permittivity of a spherical inclusion sparsely distributed in a dielectric host.

Using the same material as in the Maxwell Garnett section, the Clausius Mosotti formula has been graphed versus frequency for 3 different volume fractions: 0.4, 0.25, and 0.1.

The particle radius is 1.91  $\mu\text{m}$ . The measured data is as before.

### Clausius Mosotti Permittivity [ f=0.4 ]

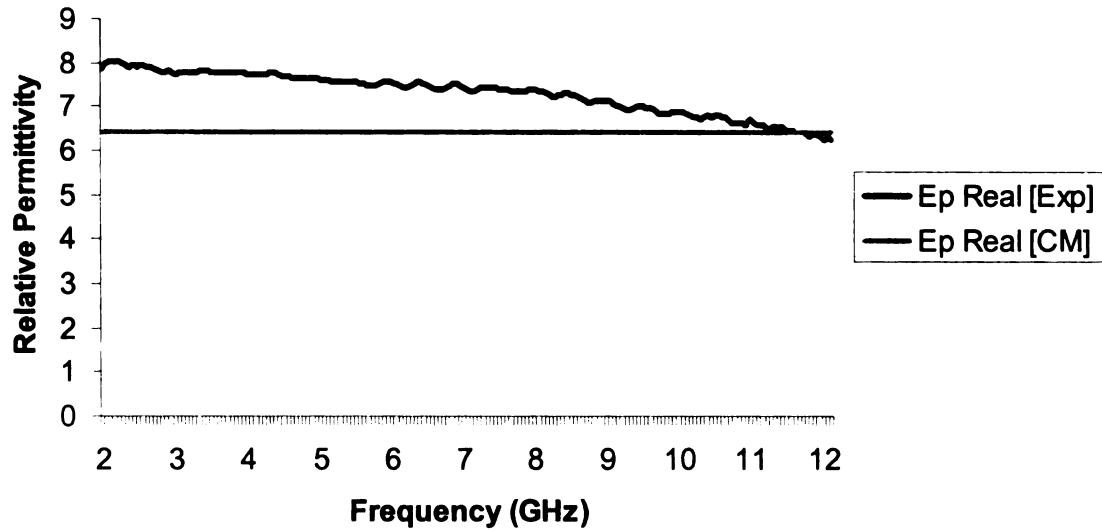


Figure 4.2.2: Clausius Mosotti calculated permittivity graphed with measured permittivity of a sample with volume fraction  $f=0.4$ .

### Clausius Mosotti Permittivity [ f=0.25 ]

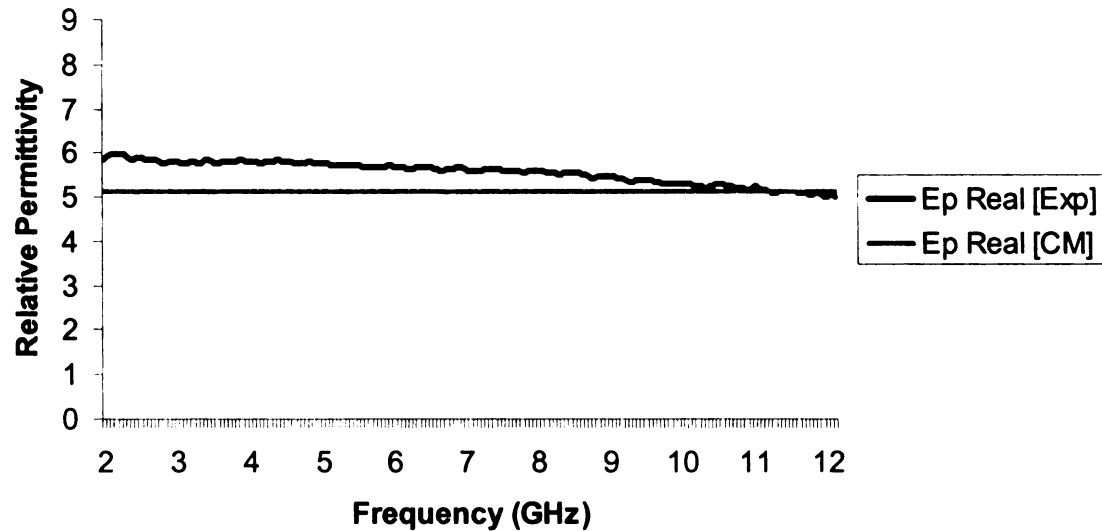


Figure 4.2.3: Clausius Mosotti calculated permittivity graphed with measured permittivity of a sample with volume fraction  $f=0.25$ .

### Clausius Mosotti Permittivity [ $f=0.1$ ]

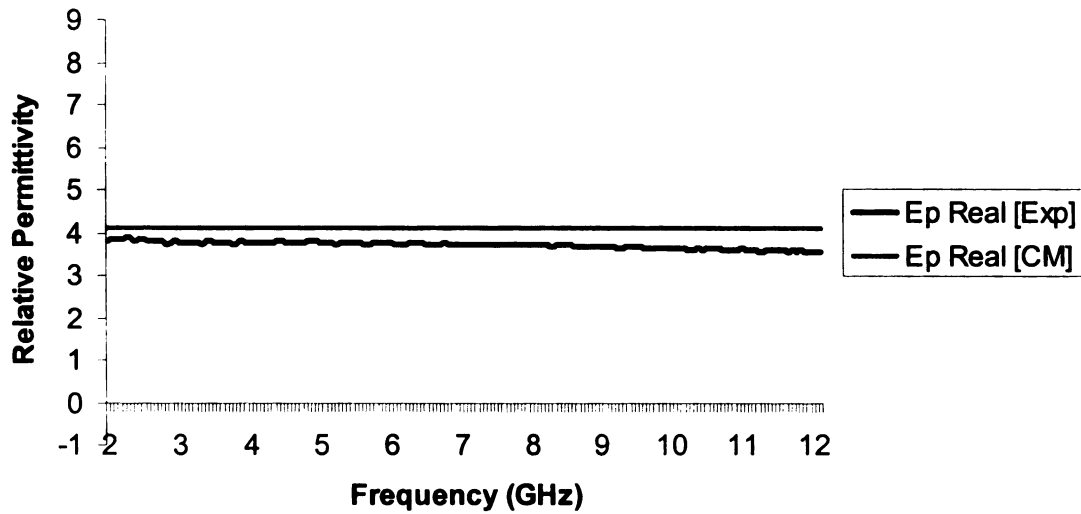


Figure 4.2.4: Clausius Mosotti calculated permittivity graphed with measured permittivity of a sample with volume fraction  $f=0.1$ .

Similar to Maxwell Garnett results, the Clausius Mosotti formula seems to be more accurate as the volume fraction decreases. Although this formulation seems to be a less averaged approach to modeling effective permittivity as the Maxwell Garnett by replacing each particle with a dipole, it still does not account for any interaction between particles. Therefore as the inclusions are more sparsely distributed, the more accurate the prediction can be. The following three figures show the results from Clausius Mosotti and Maxwell Garnett together for purposes of comparison.

### Maxwell Garnett, Clausius Mosotti, and Experimental Permittivity for $f=0.4$

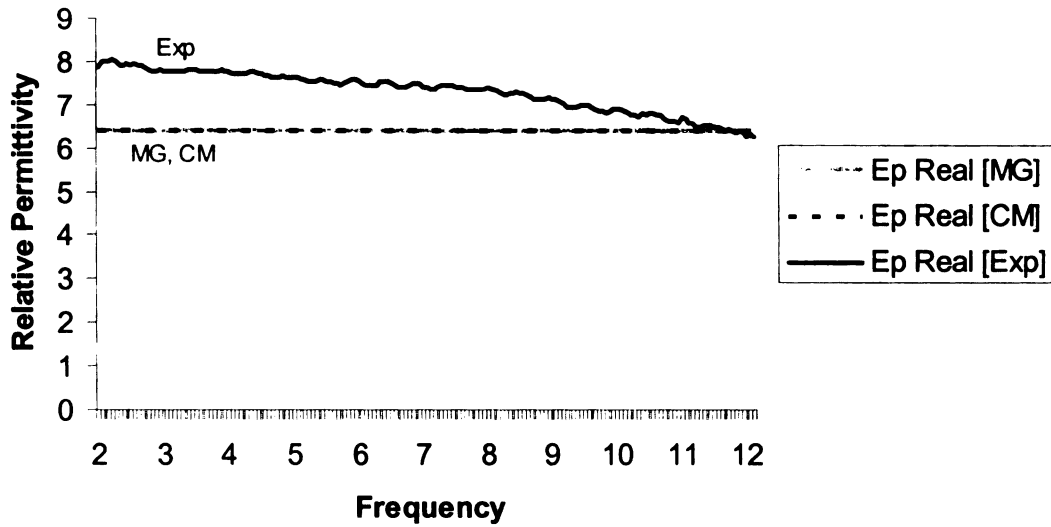


Figure 4.2.5: Comparison of Clausius Mosotti to Maxwell Garnett and Experimental data for  $f=0.4$

### Maxwell Garnett, Clausius Mosotti, and Experimental Permittivity for $f=0.25$

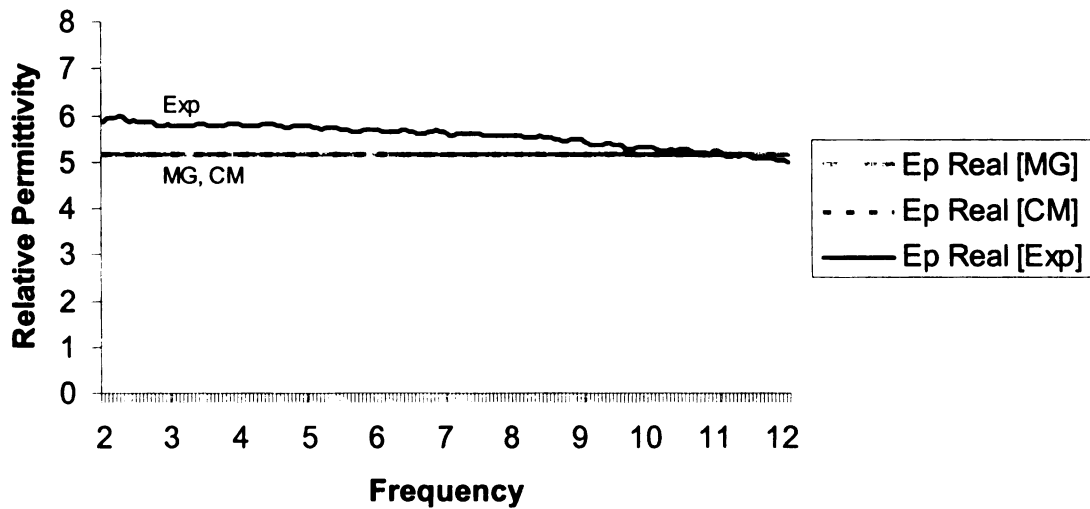


Figure 4.2.6: Comparison of Clausius Mosotti to Maxwell Garnett and Experimental data for  $f=0.25$ .

## Maxwell Garnett, Clausius Mosotti, and Experimental Permittivity for $f=0.1$

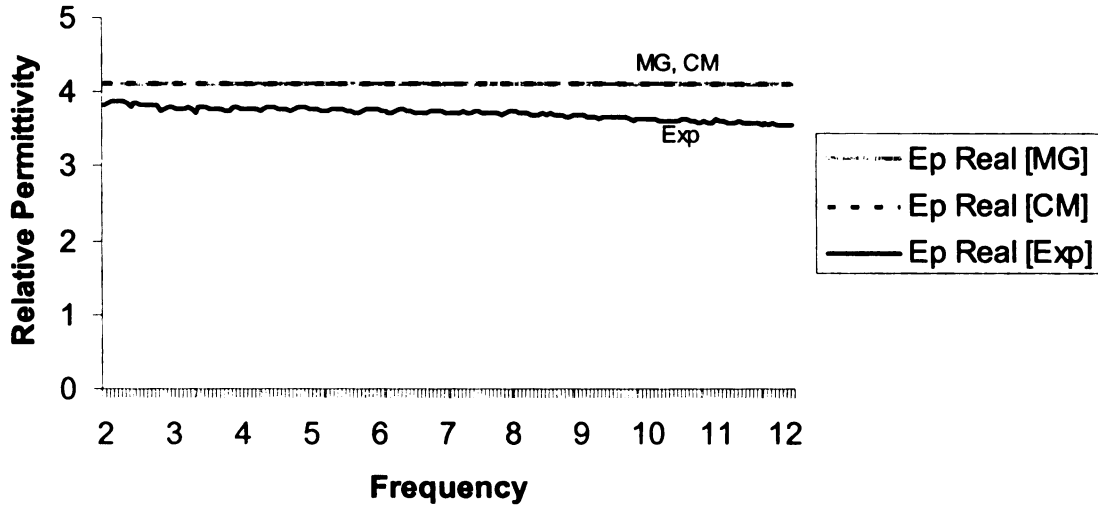


Figure 4.2.7: Comparison of Clausius Mosotti to Maxwell Garnett and Experimental data for  $f=0.1$ .

Figures 4.2.5, 4.2.6, and 4.2.7 show that for the geometry used here the Clausius Mosotti and Maxwell Garnett formulations predict the same effective permittivity. This led to further investigation into the two equations. When the polarizability is as given in equation (4.2.10) and the number density  $N$  is represented as in equation (4.2.11) the Clausius Mosotti formula can be shown to be exactly the same as the Maxwell Garnett equation.

$$N = f / V \quad (4.2.11)$$

Inserting (4.2.10) and (4.2.11) into equation (4.2.8) for effective permittivity we get the following formula.

$$\epsilon_{eff} = \epsilon_e \frac{3 + 2(f/V)3\epsilon_e V [(\epsilon_i - \epsilon_e)/(\epsilon_i + 2\epsilon_e)](1/\epsilon_e)}{3 - (f/V)3\epsilon_e V [(\epsilon_i - \epsilon_e)/(\epsilon_i + 2\epsilon_e)](1/\epsilon_e)} \quad (4.2.12)$$

Dropping out like terms, dividing by 3 and multiplying by  $(\varepsilon_i + 2\varepsilon_e)/(\varepsilon_i + 2\varepsilon_e)$  we get equation (4.2.13).

$$\varepsilon_{eff} = \varepsilon_e \frac{\varepsilon_i + 2\varepsilon_e - f(\varepsilon_i - \varepsilon_e) + 3f(\varepsilon_i - \varepsilon_e)}{\varepsilon_i + 2\varepsilon_e - f(\varepsilon_i - \varepsilon_e)} \quad (4.2.13)$$

Realizing the first three terms of the numerator in (4.2.13) are equal to the denominator, this equation can be further simplified to give equation (4.2.14) which is exactly the same as equation (4.1.7) defined in the previous section as the Maxwell Garnett formula.

$$\varepsilon_{eff} = \varepsilon_e + 3\varepsilon_e f \frac{(\varepsilon_i - \varepsilon_e)}{\varepsilon_i + 2\varepsilon_e - f(\varepsilon_i - \varepsilon_e)} \quad (4.2.14)$$

This explains why the effective permittivity found using the Maxwell Garnett and the Clausius Mosotti yield the same results for the dielectric spheres.

### **4.3 – Bruggeman Permittivity**

The Bruggeman formula for the homogenization of a mixture is widely used the electromagnetics. It is known for different names depending on where it is used; in the remote sensing community it goes under the names Polder-van Santen and the de Loor formula. It is also known as the Böttcher formula or in materials science it is often referred to as the effective medium model [20]. This model analyzes the polarization of the mixture as a function of the environment equally as much as the inclusions. The Bruggeman philosophy is represented in equation (4.3.1) where  $N$  is the number of isotropic phases. For the case in this thesis  $N=2$ ; one is for the environment and the other for the spherical inclusions.

$$\sum_{j=1}^N f_j \frac{\epsilon_j - \epsilon_{eff}}{\epsilon_j + 2\epsilon_{eff}} = 0 \quad (4.3.1)$$

Letting  $j=1$  represent the environment phase  $\epsilon_e = \epsilon_1$ , and the volume fraction  $f_1 = (1-f)$ .

Now for  $j=2$ , the inclusion phase permittivity will be  $\epsilon_i = \epsilon_2$  and the volume fraction  $f_2=f$ .

Now writing out the summation for these two terms we get the following formula.

$$(1-f) \frac{\epsilon_e - \epsilon_{eff}}{\epsilon_e + 2\epsilon_{eff}} + f \frac{\epsilon_i - \epsilon_{eff}}{\epsilon_i + 2\epsilon_{eff}} = 0 \quad (4.3.2)$$

Bringing the first term in (4.3.2) over to the right side of the equation and multiplying out the denominators we get equation (4.3.3).

$$f(\epsilon_i - \epsilon_{eff})(\epsilon_e + 2\epsilon_{eff}) = (1-f)(\epsilon_e - \epsilon_{eff})(\epsilon_i + 2\epsilon_{eff}) \quad (4.3.3)$$

This can be multiplied out and put in the form of a quadratic equation with the following coefficients.

$$\begin{aligned} \epsilon_{eff}^2 A + \epsilon_{eff} B + C &= 0 \\ A &= -2 \\ B &= 2f\epsilon_i - 3f\epsilon_e + f\epsilon_i + 2\epsilon_e - \epsilon_i \\ C &= \epsilon_i\epsilon_e \end{aligned} \quad (4.3.4)$$

Solving the quadratic formula represented by (4.3.4) and taking the non-negative result gives the effective permittivity of the mixture. This was done for the material of hexaferrite inclusions with a relative permittivity of 16, and environment with relative permittivity of 3.5 for all three volume fractions; 0.4, 0.25, and 0.1.

### Bruggeman Effective Permittivity [f=0.4]

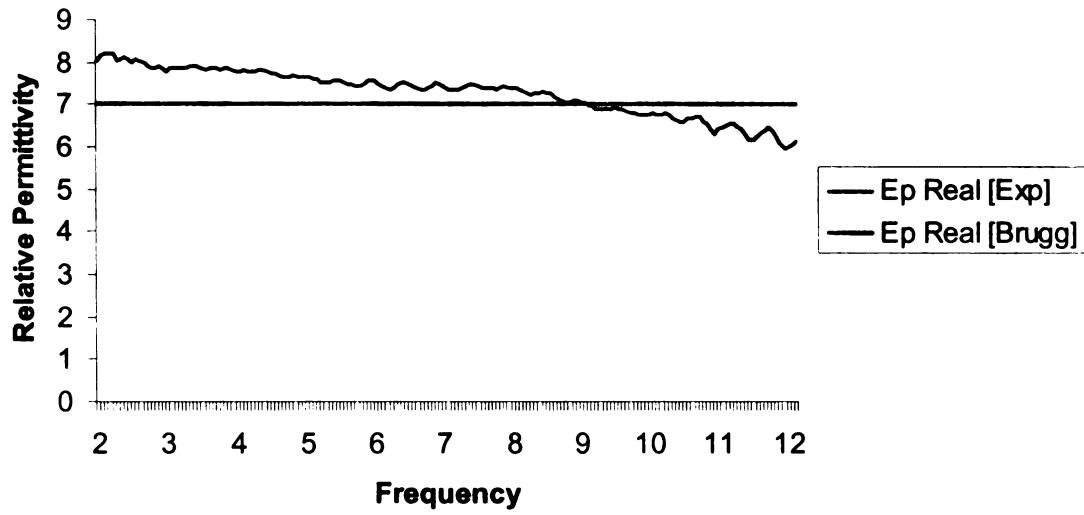


Figure 4.3.1: Bruggeman calculated permittivity graphed with measured permittivity of a sample with volume fraction  $f=0.4$ .

### Bruggeman Effective Permittivity [f=0.25]

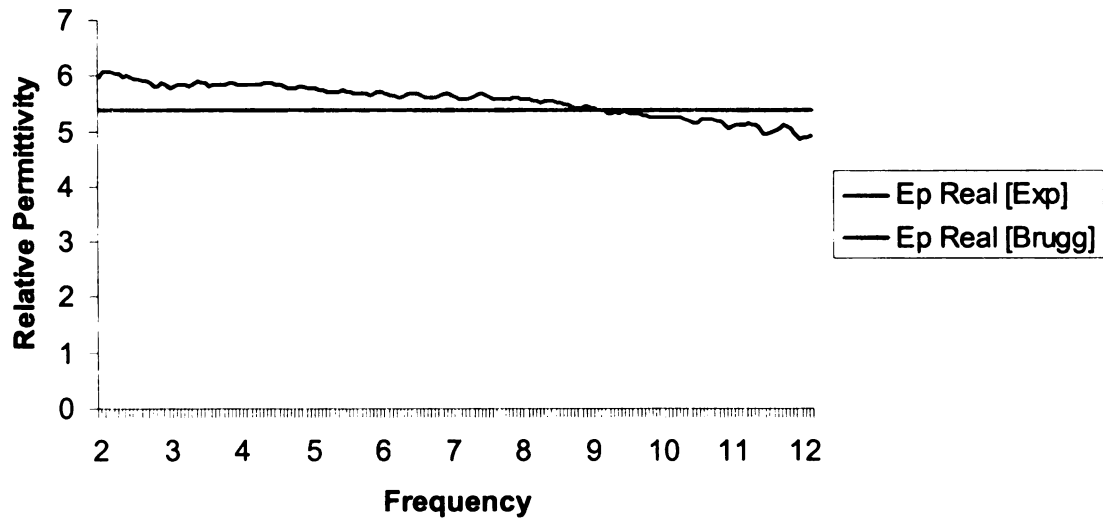


Figure 4.3.2: Bruggeman calculated permittivity graphed with measured permittivity of a sample with volume fraction  $f=0.25$ .

### Bruggeman Effective Permittivity [f=0.1]

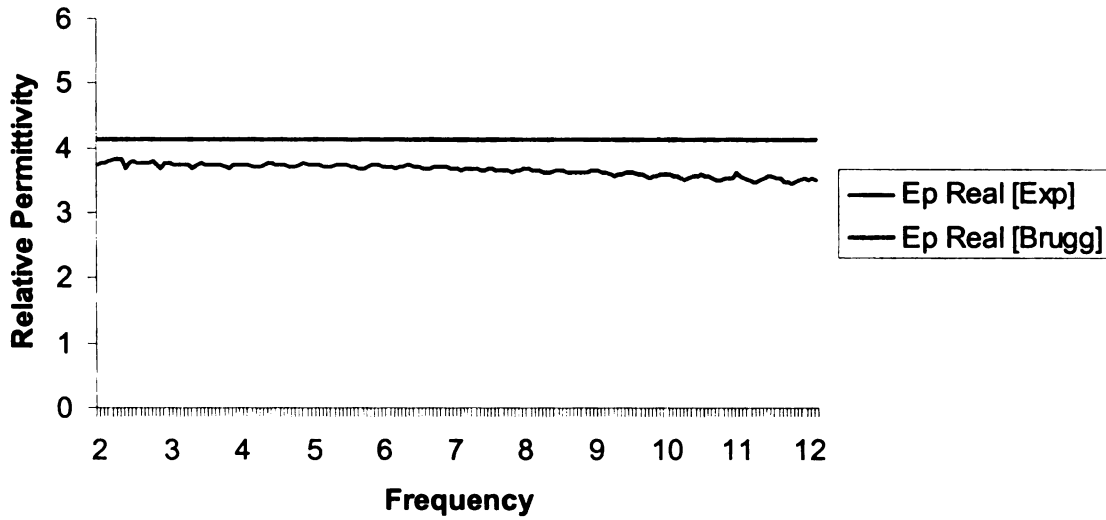


Figure 4.3.3: Bruggeman calculated permittivity graphed with measured permittivity of a sample with volume fraction  $f=0.1$ .

The results shown in Figures 4.3.1, 4.3.2, and 4.3.3 seem to be fairly close to the measured data. The following three figures compare these results using the Bruggeman formula to the results obtained from the Maxwell Garnett (Clausius Mosotti) equation.

### Maxwell Garnett, Bruggeman, and Experimental Permittivity for $f=0.4$

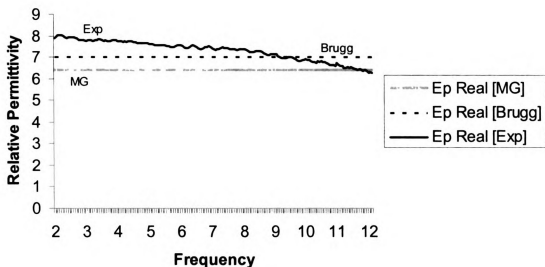


Figure 4.3.4: Maxwell Garnett, Bruggeman, and Experimental data graphed for comparison for  $f=0.4$ .

### Maxwell Garnett, Bruggeman, and Experimental Permittivity for $f=0.25$

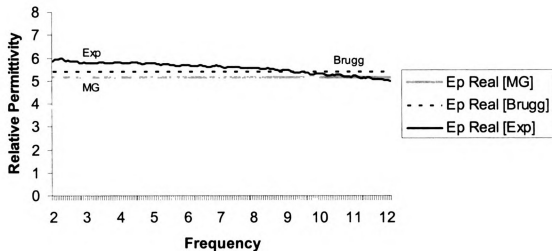


Figure 4.3.5: Maxwell Garnett, Bruggeman, and Experimental data graphed for comparison for  $f=0.25$ .

### Maxwell Garnett, Bruggeman, and Experimental Permittivity for $f=0.1$

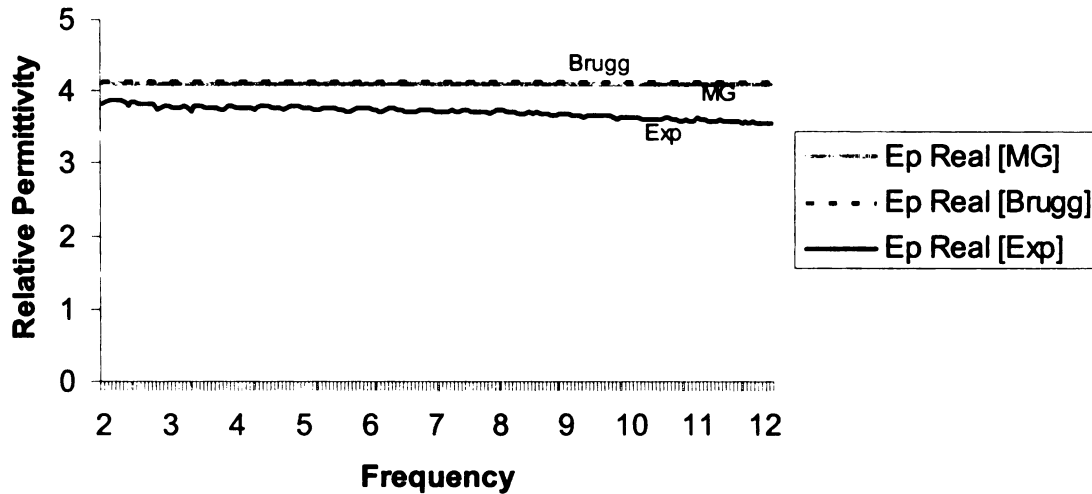


Figure 4.3.6: Maxwell Garnett, Bruggeman, and Experimental data graphed for comparison for  $f=0.1$ .

Figures 4.3.4, 4.3.5, and 4.3.6 show that the Bruggeman approximation is a little more accurate in determining the effective permittivity of a material composed of dielectric spheres dispersed throughout a matrix.

The interpretation of the Bruggeman formula, equation (4.3.2), is that the formula balances both mixing components with respect to the unknown effective medium, using the volume fraction of each component as weight giving it symmetry which is not the case for Maxwell Garnett and Clausius Mosotti whose focus is on the inclusion more than the environment [20].

#### 4.4 - Coherent Potential Permittivity

Another method for finding the effective permittivity of a mixture with spherical inclusions is the well known formula called *Coherent Potential formula* [20]. This can commonly be seen in the following form.

$$\varepsilon_{eff} = \varepsilon_e + f(\varepsilon_i - \varepsilon_e) \frac{3\varepsilon_{eff}}{3\varepsilon_{eff} + (1-f)(\varepsilon_i - \varepsilon_e)} \quad (4.4.1)$$

This can be rearranged into a quadratic formula with the coefficients

$$\begin{aligned} A &= 3 \\ B &= (1-f)(\varepsilon_i - \varepsilon_e) - 3f(\varepsilon_i - \varepsilon_e) - 3\varepsilon_e \\ C &= -\varepsilon_e(1-f)(\varepsilon_i - \varepsilon_e) \end{aligned} \quad (4.4.2)$$

The philosophy behind the approaches that led to Coherent potential mixing formulas is that one should not treat a single scatterer floating in isolation in the environment when the dipole moment and the local field are calculated. Instead, the Green's function which is used to enumerate the field of a given polarization density is taken to be that of the effective medium, not that of the background [20].

The Coherent Potential formula is derived using the quasicrystalline approximation for spherical particles embedded in a background medium. In the low frequency limit this approximation can be reduced to the following [26].

$$\overline{\hat{C}}_p(\overline{p}_1, \overline{p}_2) = \hat{c}\overline{I} \quad (4.4.3)$$

Where  $\overline{p}_1$  and  $\overline{p}_2$  are the momentum operators.

$$\hat{c} = v_0 \hat{t}_m + f \hat{t}_m \hat{c} \left[ \frac{1}{3K^2} + \frac{2}{3} jK \int_0^\infty dr r^2 [g(r) - 1] \right] \quad (4.4.4)$$

and

$$\hat{t}_m = \frac{z}{1 + z/(3K^2)} \left[ 1 + j \frac{2}{9} \frac{Ka^3 z}{1 + z/(3K^2)} \right] \quad (4.4.5)$$

$K$  is the coherent propagation constant of the effective medium,  $f = n_0 v_0$  is the volume fraction comprised of the number density multiplied by the volume of a spherical inclusion whose radius is  $a$ . The transition operator  $\hat{t}_m$  represented by equation (4.4.5) is inserted into (4.4.4) and gives the following.

$$\hat{c} = \frac{v_0 z}{1 + z(1-f)/(3K^2)} \left\{ 1 + j \frac{2}{9} Ka^3 \frac{z}{1 + z(1-f)/(3K^2)} \times \left[ 1 + 4\pi n_0 \int_0^\infty [g(r) - 1] \right] \right\} \quad (4.4.6)$$

The dispersion relation according to the quasicrystalline approximation is represented by equation (4.4.7) [26].

$$K^2 = k^2 + n_0 \hat{c} \quad (4.4.7)$$

Again,  $K$  is the propagation constant of the effective medium and  $k$  is the propagation constant of the background medium alone. Since this is the low frequency approximation the imaginary term, which is dependent on the particle size can be neglected and (4.4.6) reduces to its first term alone [26]. Therefore inserting the first term only of (4.4.6) into (4.4.7) and using the following representations for  $K$  and  $z$  we get equation (4.4.10) for the effective permittivity of the mixture.

$$K^2 = \varepsilon_{eff} \varepsilon_0 \omega \mu_0 \quad (4.4.8)$$

$$z = k_i^2 - k^2 = \omega^2 \mu_0 \epsilon_0 \epsilon_i - \omega^2 \mu_0 \epsilon_0 \epsilon_e \quad (4.4.9)$$

$$\epsilon_{eff} \epsilon_0 \omega \mu_0 = \omega^2 \mu_0 \epsilon_0 \epsilon_e + \frac{n_0 v_0 (\omega^2 \mu_0 \epsilon_0 \epsilon_i - \omega^2 \mu_0 \epsilon_0 \epsilon_e)}{1 + (\omega^2 \mu_0 \epsilon_0 \epsilon_i - \omega^2 \mu_0 \epsilon_0 \epsilon_e)(1-f)/(3\epsilon_{eff} \epsilon_0 \omega \mu_0)} \quad (4.4.10)$$

Here  $\epsilon_e$  and  $\epsilon_i$  are the relative permittivities of the background medium and inclusions respectively. Dropping out like terms and simplifying this equation can be further reduced to be the same as equation (4.4.1) shown above. For more detailed background Quasicrystalline Approximation and Coherent Potential please refer to Tsang, Kong, and Shin [26].

Using the same material as in the previous three sections, this effective permittivity is graphed at three volume fractions: 0.4, 0.25, and 0.1, along with the actual measured data. The following three graphs illustrate these comparisons.

### Coherent Potential Permittivity [ f=0.4 ]

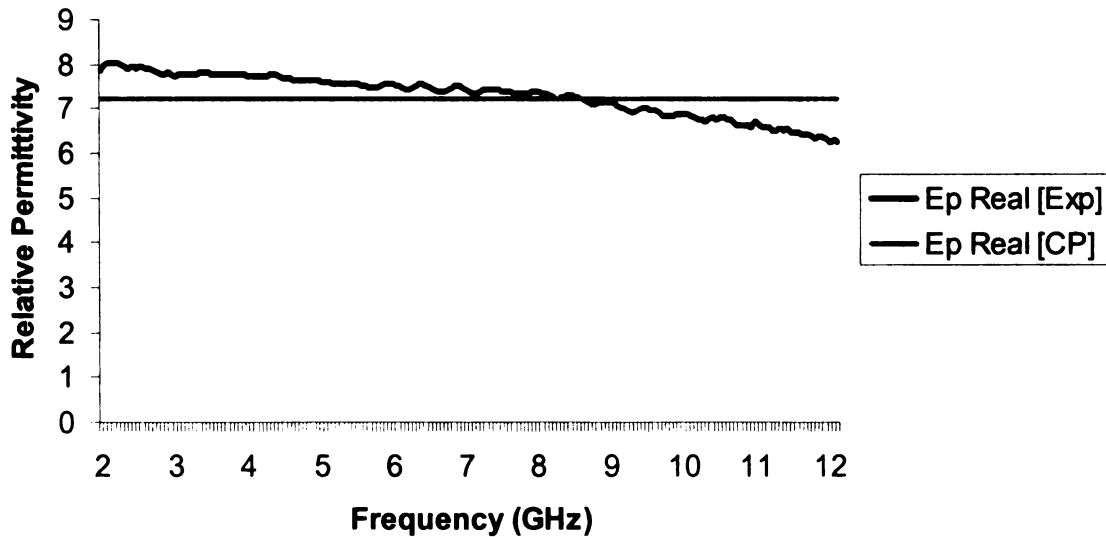


Figure 4.4.1: Coherent Potential calculated permittivity graphed with measured permittivity of a sample with volume fraction f=0.4.

### Coherent Potential Permittivity [ $f=0.25$ ]

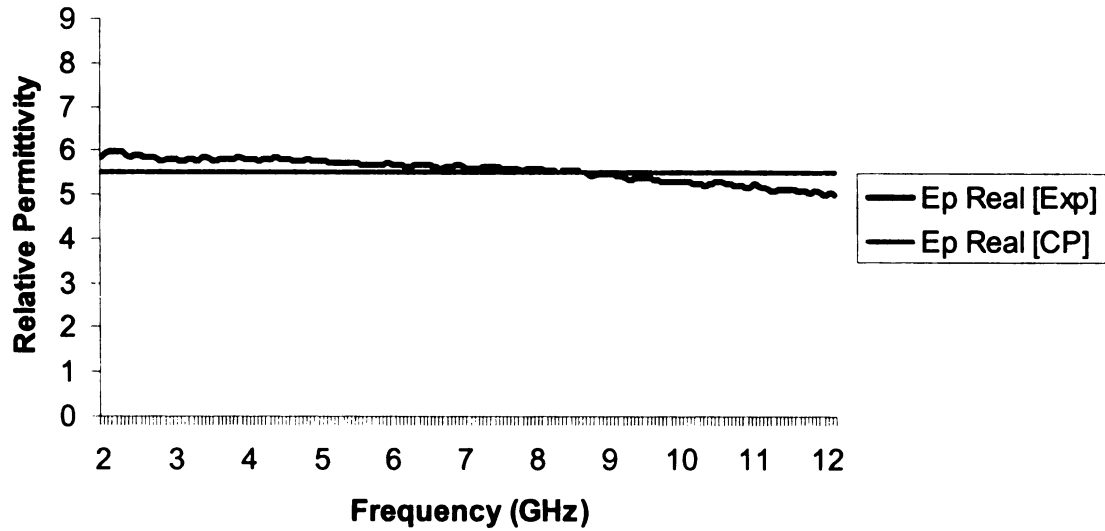


Figure 4.4.2: Coherent Potential calculated permittivity graphed with measured permittivity of a sample with volume fraction  $f=0.25$ .

### Coherent Potential Permittivity [ $f=0.1$ ]

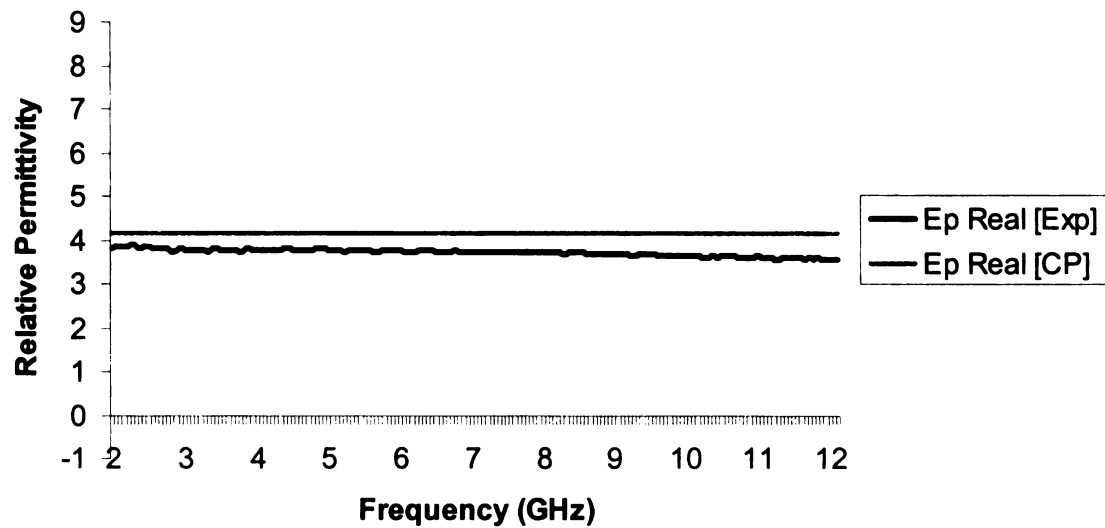


Figure 4.4.3: Coherent Potential calculated permittivity graphed with measured permittivity of a sample with volume fraction  $f=0.1$ .

A comparison of these three methods; Maxwell Garnett, Bruggeman, and Coherent Potential is shown in the following three figures along with the experimental data.

### Maxwell Garnett, Bruggeman, Coherent Potential, and Experimental Permittivity for $f=0.4$

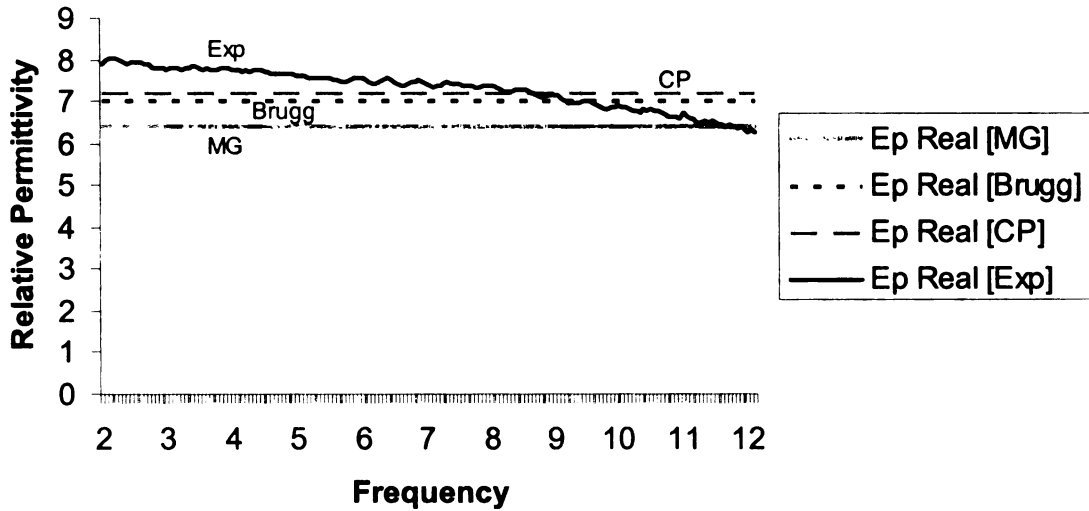


Figure 4.4.4: Maxwell Garnett, Bruggeman, Coherent Potential, and Experimental data graphed for comparison for  $f=0.4$ .

### Maxwell Garnett, Bruggeman, Coherent Potential, and Experimental Permittivity for $f=0.25$

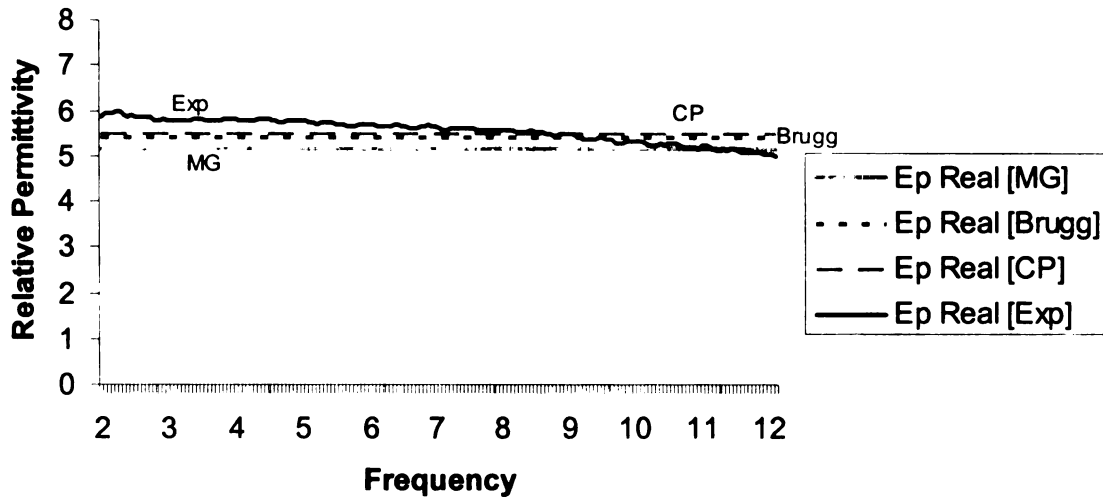


Figure 4.4.5: Maxwell Garnett, Bruggeman, Coherent Potential, and Experimental data graphed for comparison for  $f=0.25$ .

### Maxwell Garnett, Bruggeman, Coherent Potential, and Experimental Permittivity for $f=0.4$

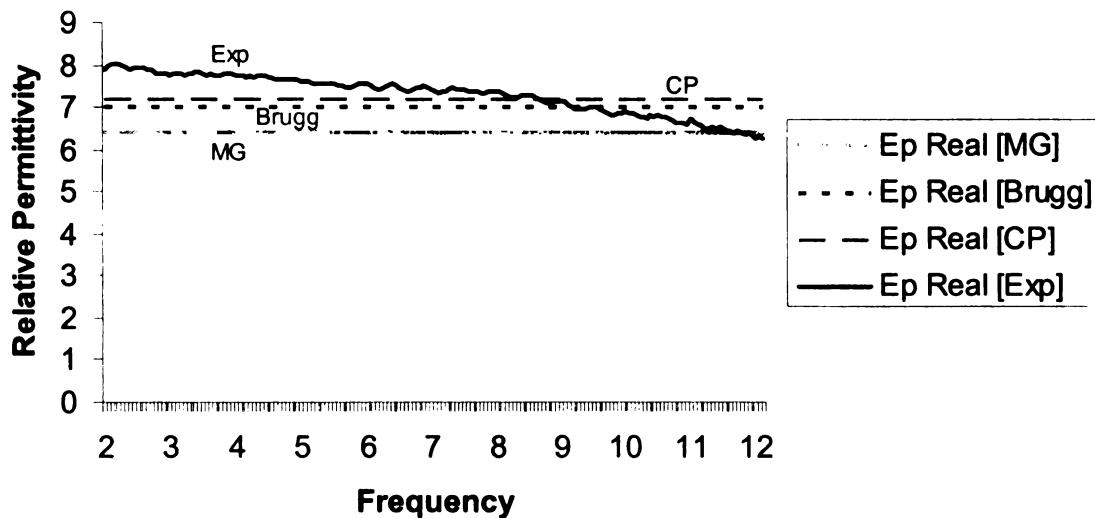


Figure 4.4.6: Maxwell Garnett, Bruggeman, Coherent Potential, and Experimental data graphed for comparison for  $f=0.4$ .

Figures 4.4.4, 4.4.5, and 4.4.6 show that although the other two methods for determining effective permittivity seemed to be relatively accurate, the Coherent Potential equation seems to be most accurate for all three volume fractions of the hexaferrite mixture.

#### **4.5 - Maxwell Garnett Permeability**

By duality, the electrostatic and magnetostatic formulations obey the same conditions for a given geometry [12] subject to appropriate boundary conditions. Therefore, given the spherical geometry of the inclusions, the permeability could be found using Maxwell Garnett formulation. The derivation would be the same as for permittivity [10], except rather than the electric displacement being related to the electric field as in (4.5.1), the flux density is related to the magnetic field intensity as in (4.5.2).

$$\langle \bar{D} \rangle = \epsilon_{eff} \langle \bar{E} \rangle \quad (4.5.1)$$

$$\langle \bar{B} \rangle = \mu_{eff} \langle \bar{H} \rangle \quad (4.5.2)$$

The resulting equation is the same as for permittivity with  $\epsilon$  replaced with  $\mu$ .

$$\mu_{eff} = \mu_e + 3f\mu_e \frac{(\mu_i - \mu_e)}{\mu_i + 2\mu_e - f(\mu_i - \mu_e)} \quad (4.5.3)$$

Equation (4.5.3) is graphed using the same hexaferrite sample as previous sections. The relative permeability of the inclusions  $\mu_i$  is 10, and the relative permeability of the non-magnetic environment  $\mu_e$  is 1. This data is graphed against the measured values for permeability at volume fractions 0.4, 0.25, and 0.1 respectively.

### Maxwell Garnett Permeability [ f=0.4 ]

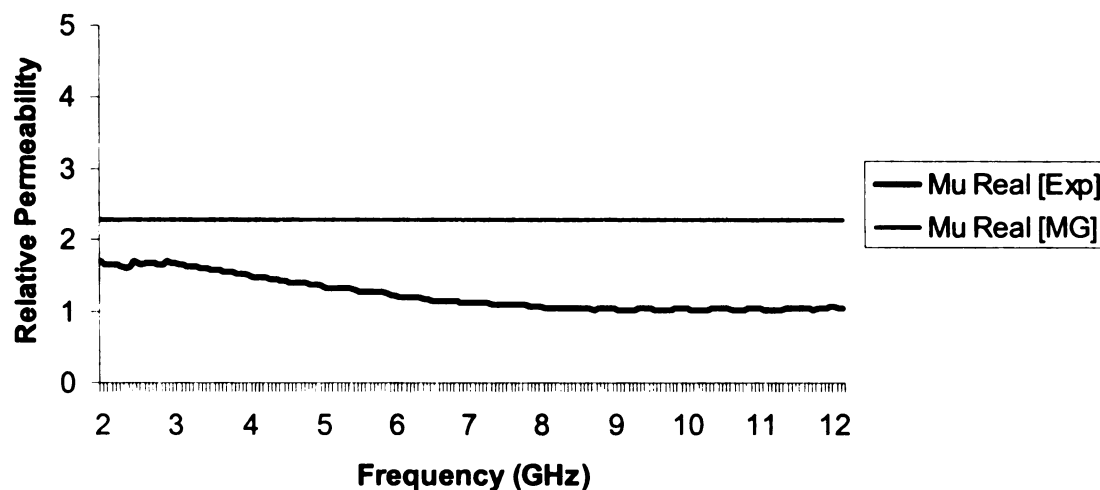


Figure 4.5.1: Maxwell Garnett calculated permeability graphed with measured permittivity of a sample with volume fraction  $f=0.4$ .

### Maxwell Garnett Permeability [ f=0.25 ]

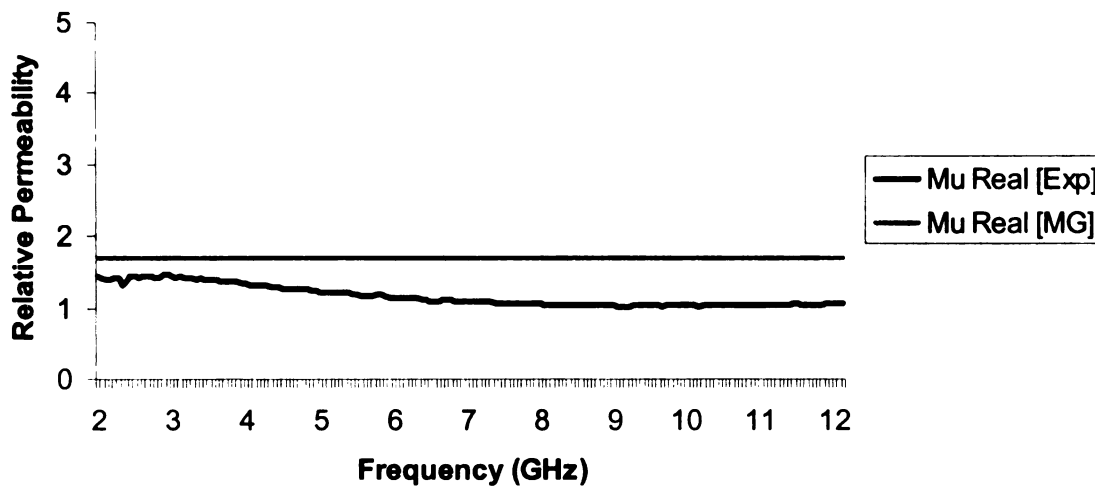


Figure 4.5.2: Maxwell Garnett calculated permeability graphed with measured permittivity of a sample with volume fraction  $f=0.25$ .

### Maxwell Garnett Permeability [ $f=0.1$ ]

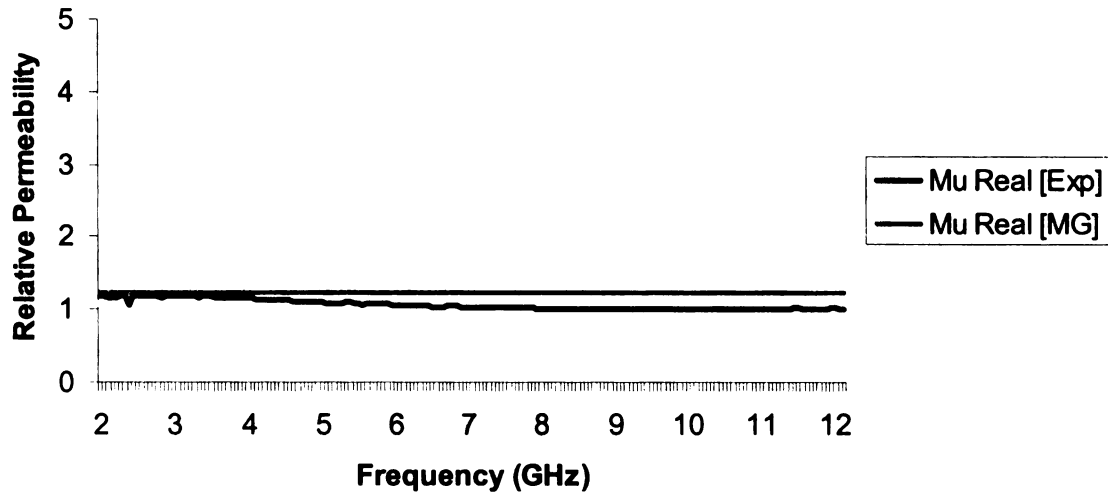


Figure 4.5.3: Maxwell Garnett calculated permeability graphed with measured permittivity of a sample with volume fraction  $f=0.1$ .

Inspecting the measured values, it is seen that the real permeability goes to 1 at frequencies above 6 GHz and becomes non-magnetic. The hexaferrite sample used in this thesis was chosen because ferrimagnetic materials can stay magnetic up to higher frequencies than other magnetic materials. However, Maxwell Garnett's theory is based on permittivities and lower frequencies and did not need to take this change into account. Therefore comparison of the calculated data and the measured data should be focused on the lower frequencies. It is not entirely accurate in finding the effective permeability, which is not surprising because of the simplicity of Maxwell Garnett's equation and the complexity of magnetism. However, upon comparison with the other classical methods to be seen in the next few sections, this approach is much more accurate than Bruggeman and Coherent Potential for finding the effective permeability of our hexaferrite sample.

#### 4.6 – Bruggeman Permeability

The Clausius Mosotti formula was found to be the same as Maxwell Garnett using this geometry for permittivity and therefore will not be demonstrated for permeability since it will only yield the same results for permeability as the previous section. However, applying the concept of duality and attempting to replace the permittivity entries with permeability in the Bruggeman equation derived in section 4.3, we get the following quadratic equation. Again, this is for a two-phase mixture, with the inclusion phase being that of magnetic spherical particles dispersed in a non-magnetic medium.

$$\begin{aligned}\mu_{eff}^2 A + \mu_{eff} B + C &= 0 \\ A &= -2 \\ B &= 2f\mu_i - 3f\mu_e + f\mu_i + 2\mu_e - \mu_i \\ C &= \mu_i\mu_e\end{aligned}\tag{4.6.1}$$

Solving (4.6.1) and taking the non-negative result will give the Bruggeman effective permeability for a mixture of this geometry. This was done for the mixture with an environment of permeability 1, and the hexaferrite particle with a permeability of 10 and graphed with measured data for all three volume fractions; 0.4, 0.25, and 0.1.

### Bruggeman Effective Permeability [f=0.4]

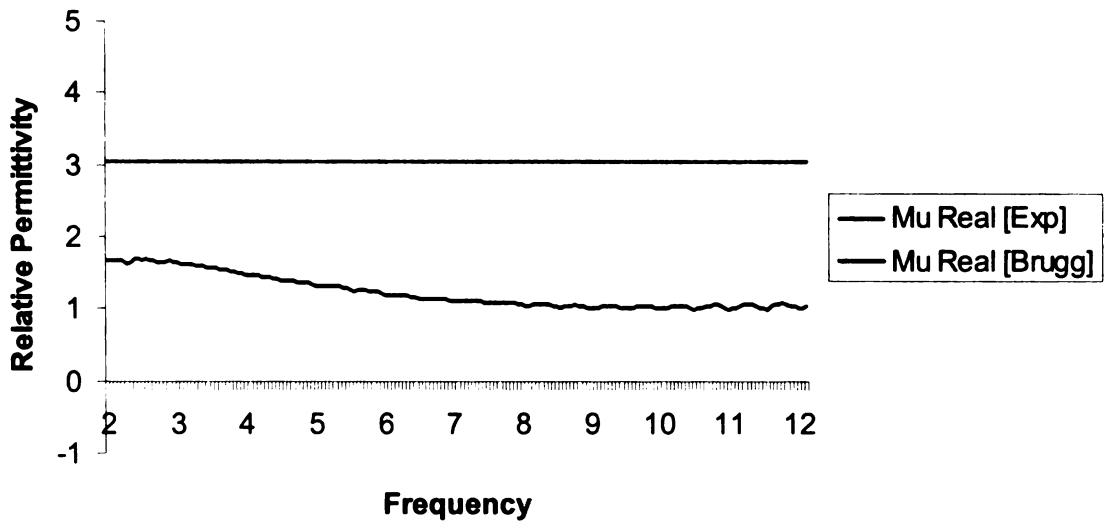


Figure 4.6.1: Bruggeman calculated permeability graphed with measured permeability of the sample with volume fraction  $f=0.4$ .

### Bruggeman Effective Permeability [f=0.25]

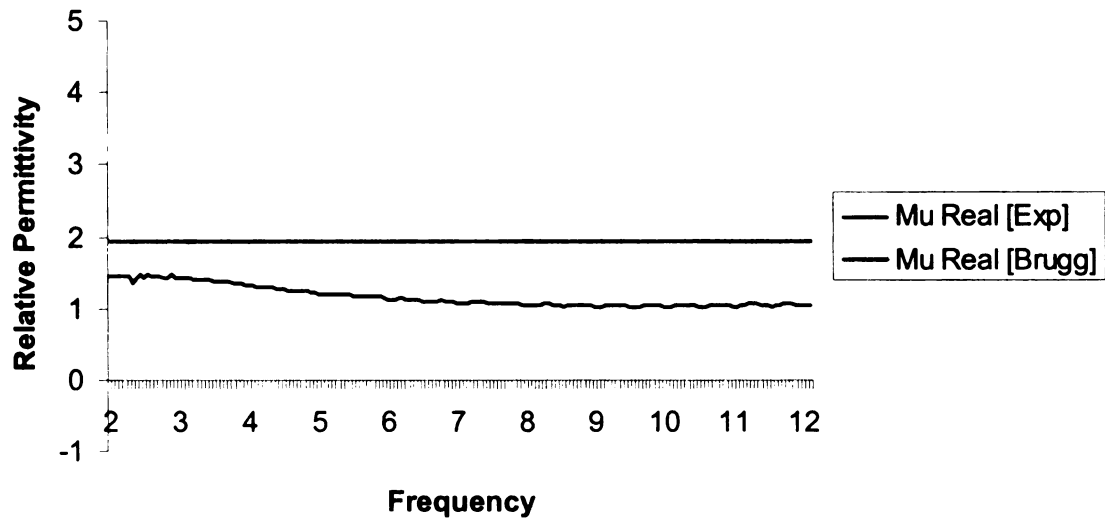


Figure 4.6.2: Bruggeman calculated permeability graphed with measured permeability of the sample with volume fraction  $f=0.25$ .

## Bruggeman Effective Permeability [f=0.1]

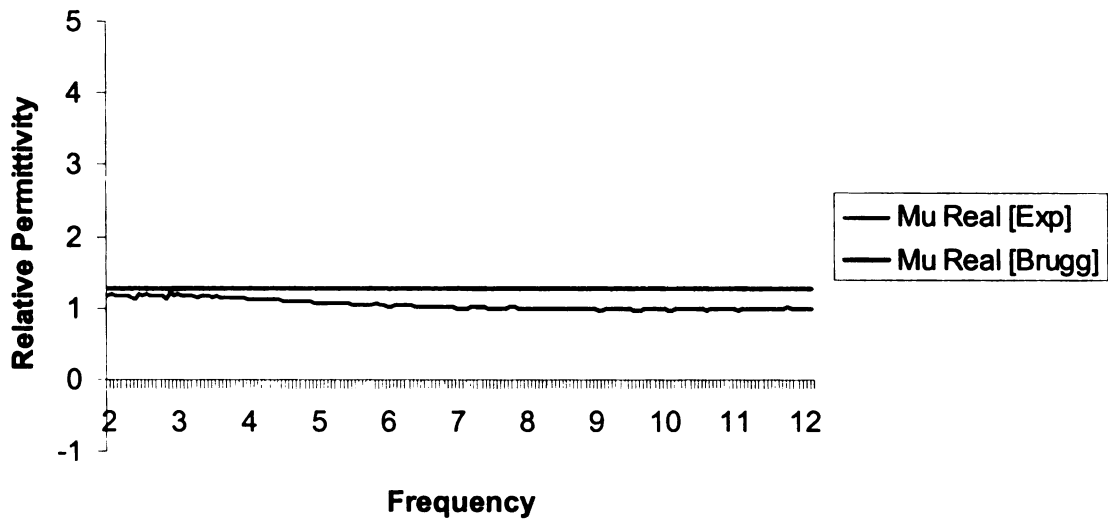


Figure 4.6.3: Bruggeman calculated permeability graphed with measured permeability of the sample with volume fraction  $f=0.1$ .

This prediction does not seem to be very accurate until the volume fraction is down to 0.1 where it is hardly exhibiting any magnetic characteristics. For comparison, this data will be graphed again with Maxwell Garnett and experimental data to see which is a better model for permeability.

### Maxwell Garnett, Bruggeman, and Experimental Permeability for $f=0.4$

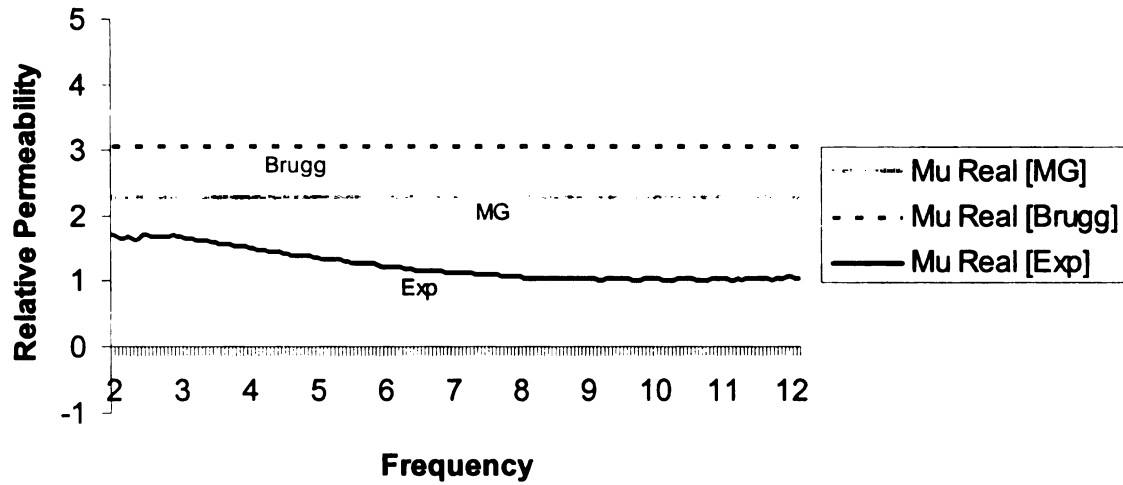


Figure 4.6.4: Maxwell Garnett, Bruggeman, and Experimental data graphed for comparison for  $f=0.4$ .

### Maxwell Garnett, Bruggeman, and Experimental Permeability for $f=0.25$

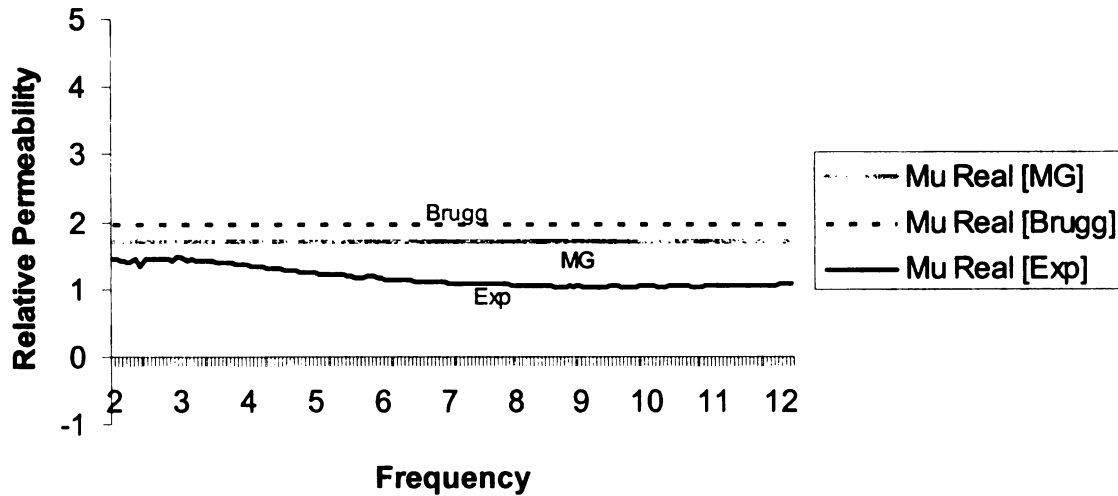


Figure 4.6.5: Maxwell Garnett, Bruggeman, and Experimental data graphed for comparison for  $f=0.25$ .

## Maxwell Garnett, Bruggeman, and Experimental Permeability for $f=0.1$

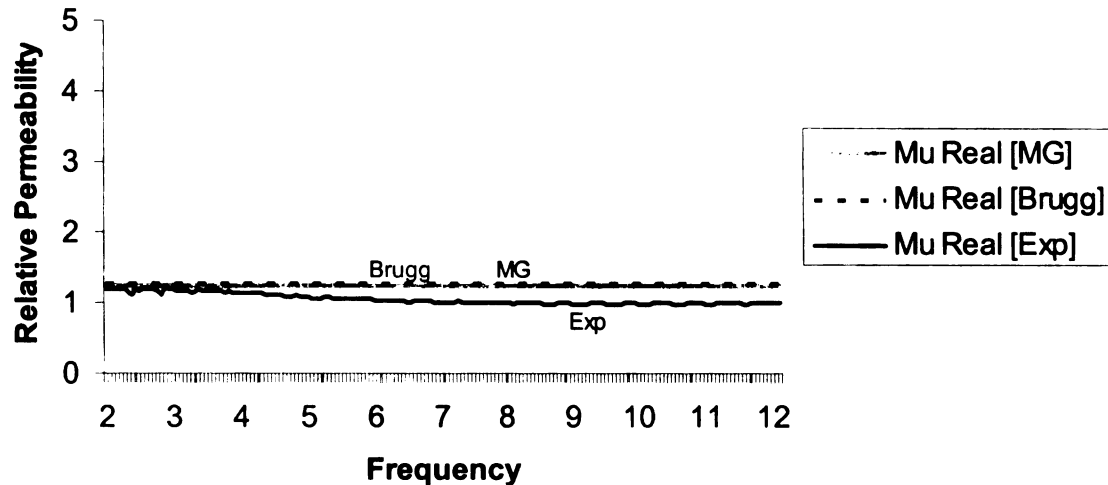


Figure 4.6.6: Maxwell Garnett, Bruggeman, and Experimental data graphed for comparison for  $f=0.1$ .

Figures 4.6.4, 4.6.5, and 4.6.6 make it apparent that the Maxwell Garnett formula is a little closer to the measured values as the volume fraction is increased. This is most likely because the Maxwell Garnett equation focuses more on the inclusion being the result of effective permeability, whereas the Bruggeman formula is symmetric and places equal importance on the inclusions as it does the environment based on its volume fractions. In magnetism, the particle to particle interaction needs to be handled more carefully and therefore the inclusions dispersed in a non-magnetic medium definitely dominate how the mixture's magnetic characteristics will turn out.

#### 4.7 - Coherent Potential Permeability

Again, using duality to try to find the permeability of a mixture using the coherent potential formula for effective permittivity described earlier we have the following plots for mixtures of volume fractions 0.4, 0.25, and 0.1 respectively.

$$\mu_{eff} = \mu_e + f(\mu_i - \mu_e) \frac{3\mu_{eff}}{3\mu_{eff} + (1-f)(\mu_i - \mu_e)} \quad (4.7.1)$$

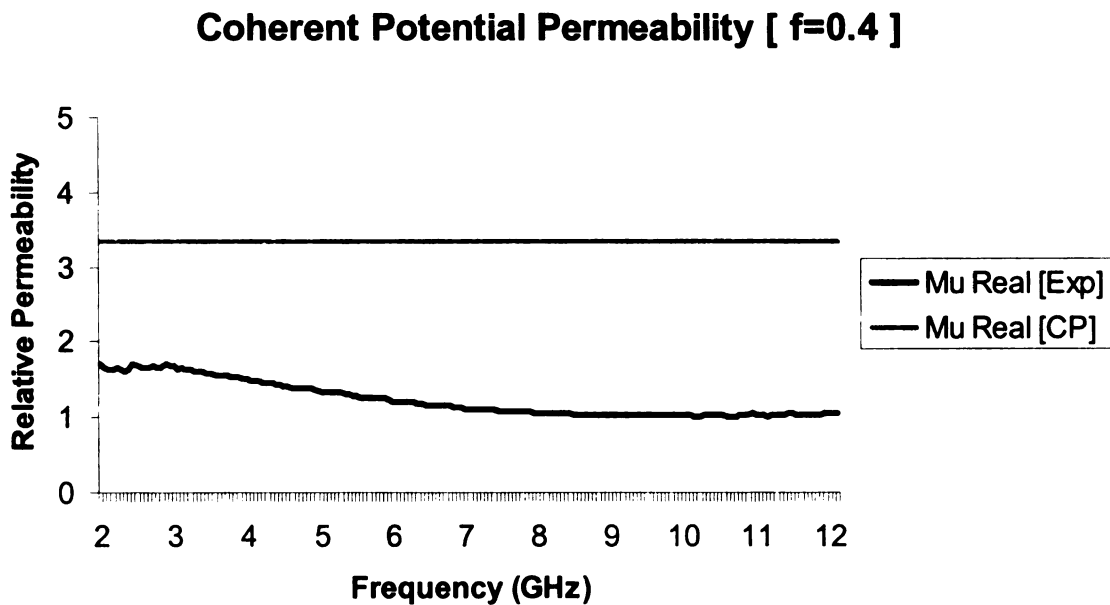


Figure 4.7.1: Coherent Potential calculated permeability graphed with measured permittivity of a sample with volume fraction  $f=0.4$ .

### Coherent Potential Permeability [ $f=0.25$ ]

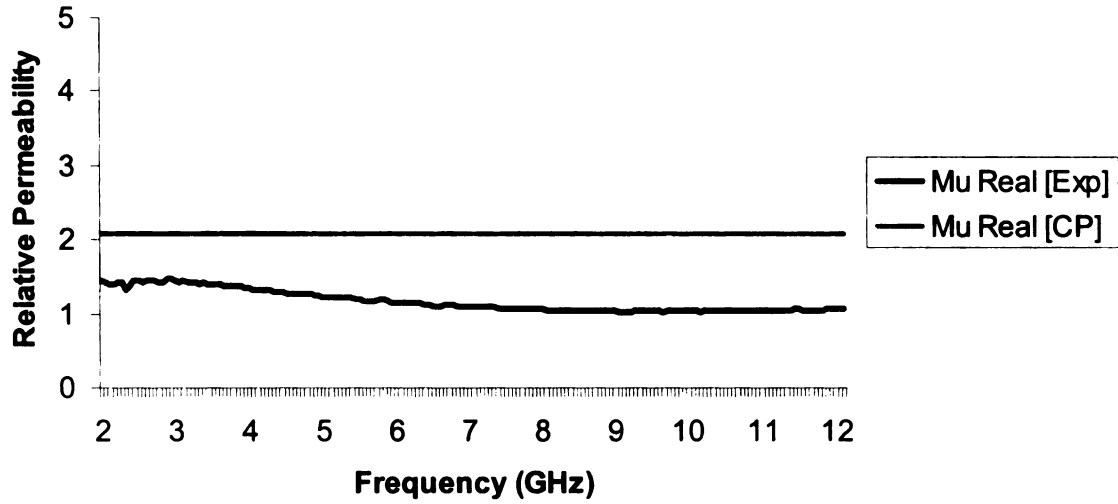


Figure 4.7.2: Coherent Potential calculated permeability graphed with measured permittivity of a sample with volume fraction  $f=0.25$ .

### Coherent Potential Permeability [ $f=0.1$ ]

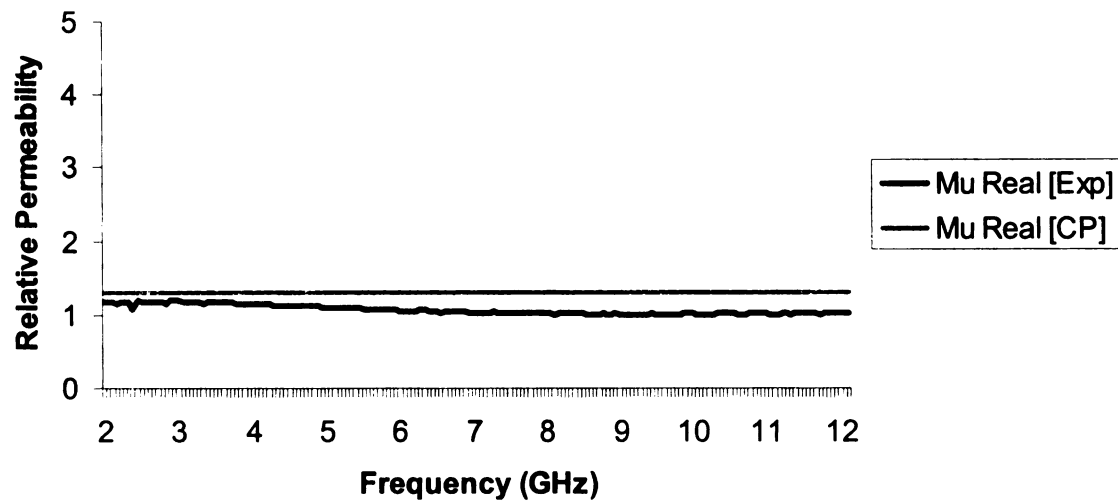


Figure 4.7.3: Coherent Potential calculated permeability graphed with measured permittivity of a sample with volume fraction  $f=0.1$ .

Similar to the Bruggeman equation, the Coherent Potential formulation seems to be close when the mixture is barely magnetic with a relative permeability of one, but does not seem to be very close for higher volume fractions than 0.1.

Finally, the results from Figures 4.7.1, 4.7.2, and 4.7.3 are graphed with the results from the permeability calculation of Maxwell Garnett, and Clausius Mosotti for purposes of comparison.

### Maxwell Garnett, Bruggeman, and Experimental Permeability for $f=0.4$

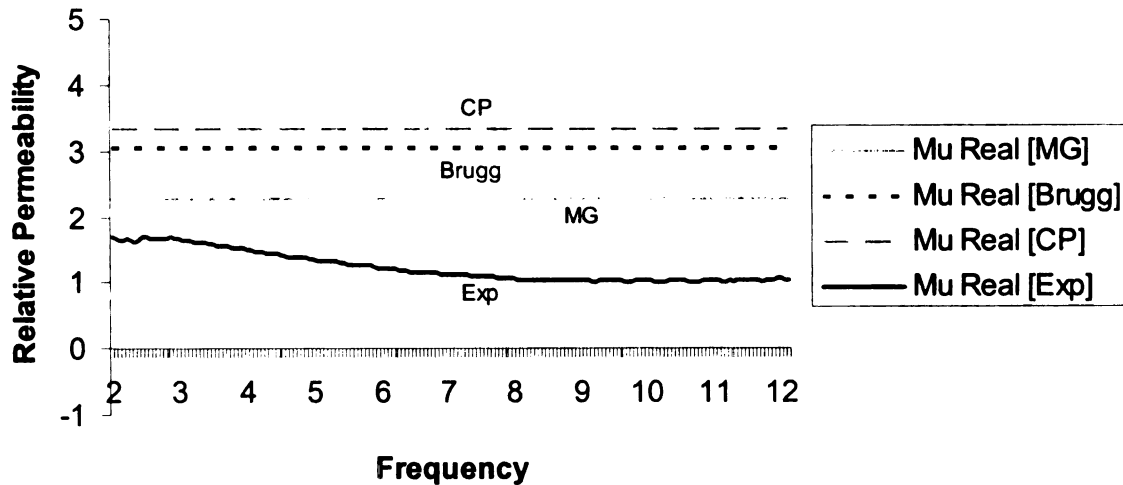


Figure 4.7.4: Maxwell Garnett, Bruggeman, Coherent Potential and Experimental data graphed for comparison when  $f=0.4$ .

### Maxwell Garnett, Bruggeman, and Experimental Permeability for $f=0.25$

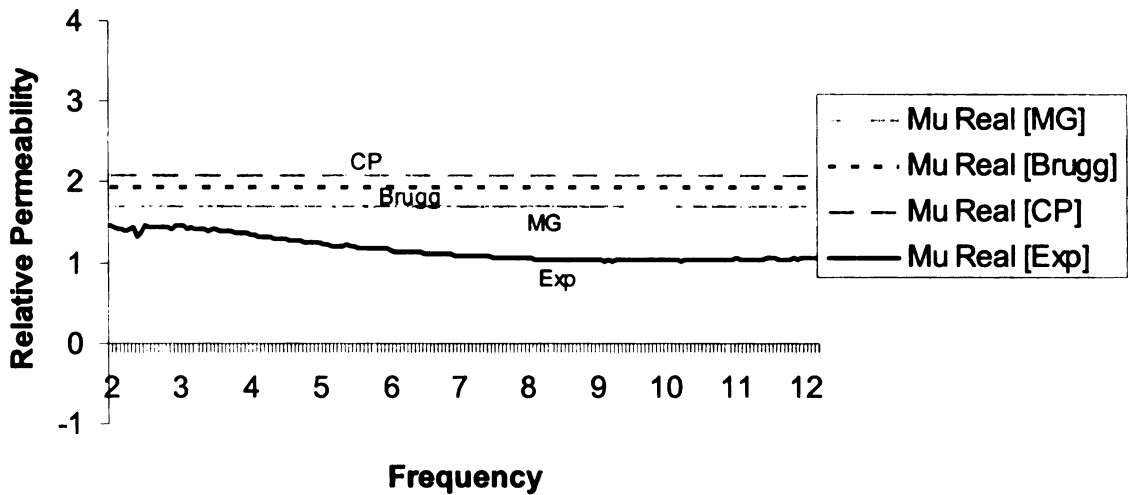


Figure 4.7.5: Maxwell Garnett, Bruggeman, Coherent Potential and Experimental data graphed for comparison when  $f=0.25$ .

### Maxwell Garnett, Bruggeman, Coherent Potential and Experimental Permeability for $f=0.1$

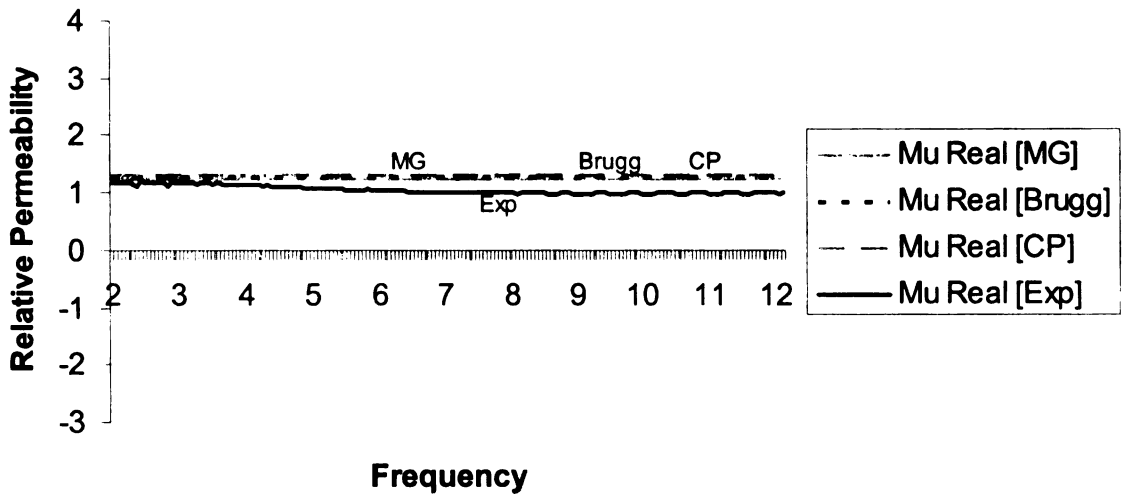


Figure 4.7.6: Maxwell Garnett, Bruggeman, Coherent Potential and Experimental data graphed for comparison when  $f=0.1$ .

Figures 4.7.4, 4.7.5, and 4.7.6 show that Maxwell Garnett is the better approximation for effective permeability for the hexaferrite mixture used in this thesis. Again, this is probably due to the fact that the Maxwell Garnett formula focuses on how the inclusion affects the entire mixture whereas Coherent Potential and Bruggeman look at the sample as a homogenous medium.

#### **4.8 - Onsager Permeability**

The Maxwell Garnett, Clausius Mosotti, and other classical mixing approaches are considered fairly accurate for determining effective permittivity of sparsely distributed inclusions which are much smaller than a wavelength, allowing for electrostatic approximations. However, when dealing with magnetic materials where the permeability of inclusions has a real value greater than one, there is an interaction that must be realized. The presence of permanent magnetic moments means that the theories like Maxwell Garnett are inapplicable to the calculation of  $\mu_{eff}$  [19]. Onsager's theory describes the local interaction between the magnetic field and the magnetic medium which will be used to arrive to an averaged description in terms of effective dielectric and magnetic permeability [5].

One assumption is that the particles are mono-domain, and therefore dipolar interaction is negligible, and they are small in relation to wavelength. With these assumptions, it will be valid to use a quasi-static magnetic approximation for the electromagnetic fields and

their interactions with the particles [19]. Beginning by looking at the magnetization of a single particle,

$$\bar{m} = m_0 \bar{u} + \alpha \bar{F} \quad (4.8.1)$$

where  $m_0$  is the magnetic moment of the particle,  $\bar{u}$  is the unit vector in the direction of the permanent moment,  $\alpha$  is the complex magnetic polarizability, and  $\bar{F}$  is the local magnetic field. Onsager represents the local field  $\bar{F}$  as a summation of two terms: the cavity field component  $\bar{G}$  and the reaction field component  $\bar{R}$  which are obtained through boundary conditions [5]. Since the particle has a permanent magnetic moment, a inhomogeneous field is created which alters the neighboring particles' magnetic moments creating the reaction field  $\bar{R}$ . In order to find an expression for  $\bar{F}$ , the homogeneous wave equation  $\Delta\psi = 0$  can be solved for a magnetic moment in the center of a sphere of radius  $a$  surrounded by a magnetic medium with permeability  $\mu$ . General solutions to the wave equation are

$$\psi_1 = \sum_{n=0}^{\infty} \left( A_n r^n + \frac{B_n}{r^{n+1}} \right) P_n(\cos\theta) \quad (4.8.2)$$

$$\psi_2 = \sum_{n=0}^{\infty} \left( C_n r^n + \frac{D_n}{r^{n+1}} \right) P_n(\cos\theta) \quad (4.8.3)$$

after applying the boundary conditions equations, (4.8.2) and (4.8.3) become

$$\psi_1 = \frac{3m}{(2\mu + 1)r^2} \cos\theta \quad (4.8.4)$$

$$\psi_2 = \frac{m}{r^2} \cos \theta - \frac{2mr(\mu-1)}{a^3(2\mu+1)} \cos \theta \quad (4.8.5)$$

Using equation (4.8.6) to represent the magnitude of the applied field and substituting into the solutions to the wave equation (4.8.4) and (4.8.5) gives the two local Onsager fields  $\bar{F}_1$  and  $\bar{F}_2$  representing the fields inside and outside of a sphere.

$$\|\bar{H}_m\| = \frac{m\sqrt{1+3\cos^2\theta}}{r^3} \quad (4.8.6)$$

$$\bar{F}_1 = \frac{3\mu}{2\mu+1} \bar{H}_m \quad \text{for } r > a \quad (4.8.7)$$

$$\bar{F}_2 = \bar{H}_m + \frac{2(\mu-1)}{(2\mu+1)a^3} \bar{m} \quad \text{for } r < a \quad (4.8.8)$$

$\bar{F}_1$  looks a lot like the equation for the polarizability of a sphere in section 4.2 resulting from the electrostatic solution to Rayleigh scattering with permeability replacing permittivity. The resulting equation gives the cavity portion of the local Onsager field represent in equation (4.8.9). The reaction field  $\bar{R}$  which is caused by the magnetic moments within the particles is represented by equation (4.8.10). Therefore the total Onsager field as a result of the applied field  $\bar{H}$  is represented by the summation of equations (4.8.9) and (4.8.10) [5].

$$\bar{G} = \frac{3\mu}{2\mu+1} \bar{H} \quad (4.8.9)$$

$$\bar{R} = \frac{2(\mu-1)}{(2\mu+1)a^3} \bar{m} \quad (4.8.10)$$

$$\bar{F} = \bar{G} + \bar{R} \quad (4.8.11)$$

The complex polarizability  $\alpha$  is represented in its complex form by equation (4.8.12) where the real part is given by (4.8.13) and the imaginary part is (4.8.14) [24].

$$\alpha = \left( \frac{4\pi}{3} \right) a^3 (\bar{\alpha}' + j\bar{\alpha}'') \quad (4.8.12)$$

$$\bar{\alpha}' = -\left( \frac{3}{8\pi} \right) \left[ 1 - \frac{3(\sinh(2x) - \sin(2x))}{2x(\cosh(2x) - \cos(2x))} \right] \quad (4.8.13)$$

$$\bar{\alpha}'' = -\left( \frac{9}{16\pi x^2} \right) \left[ 1 - \frac{x(\sinh(2x) + \sin(2x))}{(\cosh(2x) - \cos(2x))} \right] \quad (4.8.14)$$

$\bar{\alpha}'$  is the real part of polarizability,  $\bar{\alpha}''$  is the imaginary part of the polarizability,  $a$  is the radius of the particle,  $x = a/\delta$ ,  $\delta = c/\sqrt{2\pi\sigma\omega}$  is the skin depth,  $c$  is the speed of light,  $\sigma$  is the conductivity, and  $\omega$  is the frequency. Inserting equation (4.8.11) into equation (4.8.1), we get

$$\bar{m} = m_0 \left( 1 - \frac{8\pi\bar{\alpha}(\mu-1)}{3(2\mu+1)} \right)^{-1} \hat{u} + \frac{3\mu\alpha}{2\mu+1} \left( 1 - \frac{8\pi\bar{\alpha}(\mu-1)}{3(2\mu+1)} \right)^{-1} \bar{H} \quad (4.8.15)$$

The total magnetization per unit volume is  $\bar{M} = N\langle\bar{m}\rangle$ , where  $N$  is the number of particles per unit volume. The total magnetization can then be related to the applied field by

$$\bar{M} = \frac{\mu - 1}{4\pi} \bar{H} = \frac{\bar{m}_0 \langle\hat{u}\rangle 3(2\mu + 1) + 9\mu\bar{\alpha}\bar{H}}{3(2\mu + 1) - 8\pi\bar{\alpha}(\mu - 1)} \quad (4.8.16)$$

where  $\bar{m}_0$  is the magnetic moment per unit volume and  $\langle\hat{u}\rangle$  is found by the Onsager's approach.

$$\langle\hat{u}\rangle = \frac{\mu\bar{m}_0 4\pi\alpha^3 \bar{H}}{kT[3(2\mu + 1) - 8\pi\bar{\alpha}(\mu - 1)]} \quad (4.8.17)$$

Here  $k$  is Boltzmann's constant, and  $T$  is temperature. The main point to be noted from the derivation of equation (4.8.17) is that only the cavity-field component  $\bar{G}$  has any effect on the moment, and the reaction field  $\bar{R}$  is always parallel to  $\bar{m}$  and therefore can not exert any torque on the particle [19]. Since relaxation is not instantaneous,  $\langle\hat{u}\rangle$  needs to be multiplied by an Debye relaxation time  $g(\omega)$ .

$$g(\omega) = (1 - j\omega\tau)^{-1} \quad (4.8.18)$$

Where  $\tau = \tau_0 \exp(KV/kT)$  is the orientation relaxation response function,  $K$  represents the anisotropy energy per unit volume,  $V = 4\pi\alpha^3/3$  is the volume of a single inclusion. The quantities  $\bar{\alpha}$  and  $\bar{m}_0$  are normalized values per unit volume and therefore will be multiplied by the volume fraction  $f$  of the samples. Multiplying in  $f$  and utilizing

equations (4.8.17) and (4.8.18) in equation (4.8.16), the result is an equation for the effective permeability of the mixture.

$$\frac{\mu_{eff} - 1}{4\pi} = \frac{9f\mu_{eff}(2\mu_{eff} + 1)g(\omega)\left(\frac{4\pi\alpha^3\bar{m}_0^3}{3kT}\right)}{\left[3(2\mu_{eff} + 1) - 8\pi f\bar{\alpha}(\mu_{eff} - 1)\right]^2} + \frac{9f\mu_{eff}\bar{\alpha}}{3(2\mu_{eff} + 1) - 8\pi\bar{\alpha}f(\mu_{eff} - 1)} \quad (4.8.19)$$

Equation (4.8.19) can be rewritten as a cubic equation with the following coefficients and solved for  $\mu_{eff}$ .

$$\begin{aligned} A\mu_{eff}^3 + B\mu_{eff}^2 + C\mu_{eff} + D &= 0 \\ A &= 4\left(9 + 16\pi^2 f^2 \bar{\alpha}^2 - 24\pi f\bar{\alpha}\right) \\ B &= -24\pi f\left[\bar{\alpha}(3 - 4\pi f\bar{\alpha}) + 3X g(\omega)\right] \\ C &= -3\left[32\pi^2 \bar{\alpha}^2 f^2 + 12\pi f(X g(\omega) + 3\bar{\alpha}) + 9\right] \\ D &= -\left[9 + 16\pi\bar{\alpha}f(3 + 4\pi\bar{\alpha}f)\right] \end{aligned} \quad (4.8.20)$$

Where  $X = \left(4\pi\alpha^3\bar{m}_0^2 / 3kT\right)$ , since there are going to be three solutions to this cubic equation, the physically realizable  $\mu_{eff}$  must be chosen so that  $\text{Re}\{\mu_{eff}\}$  is positive.

This formulation has been proven accurate for mono-domain ferromagnetic particles by Gadenne [19], however the ferrite material used for this thesis has a significantly smaller conductivity, and higher anisotropic constant and this relation fails because of those constraints. Although it does not work well for the hexaferrite inclusions, it is important to keep this in mind for future applications involving ferromagnetic particles.

## CHAPTER 5 - Applications

### 5.1 - Square Patch Antenna Bandwidth

A magneto-dielectric material is one with a permeability and permittivity greater than one and is the case for the hexaferrite mixture discussed throughout this thesis. A paper by Hansen and Burke [7] analyzes the bandwidth of a magneto-dielectric backed square patch antenna using its conductance and admittance. They claim that the results obtained allow one to analyze the effect of varying parameters,  $\mu$  and  $\epsilon$ , on the bandwidth using a zero-order theory. Also, that this approach will provide simple results that will only be changed slightly when looked at by more exact theories. The zero order theory states that the patch length must be as in equation (5.1.1) for resonance.

$$\frac{a}{\lambda} = \frac{1}{2\sqrt{\mu_r \epsilon_r}} \quad (5.1.1)$$

By empirical analysis, the best fit for conductance of this resonant patch is represented by

$$G \cong \frac{1}{40\sqrt{\mu_r \epsilon_r} + 170\mu_r \epsilon_r} \quad (5.1.2)$$

The characteristic admittance of a wide microstrip line is

$$Y_0 = \frac{\lambda}{2\eta\mu_r t} \quad (5.1.3)$$

where  $\lambda$  is wavelength,  $\eta = 120\pi$  is the intrinsic impedance, and  $t$  is the thickness of the substrate. For a VSWR=2, the zero order percent bandwidth of the patch antenna is defined as seen in equation (5.1.4).

$$BW = \frac{1}{\sqrt{2Q}} \quad (5.1.4)$$

where

$$Q = \frac{\pi Y_0}{4G} \quad (5.1.5)$$

Using this formulation one will be able to predict the bandwidth of a patch antenna by using the parameters,  $\mu_r$  and  $\epsilon_r$ , of the substrate. Figure 5.1.1 and Figure 5.1.2 illustrate this theory for a material with varying permeability and permittivity at a center frequency of 1 GHz.

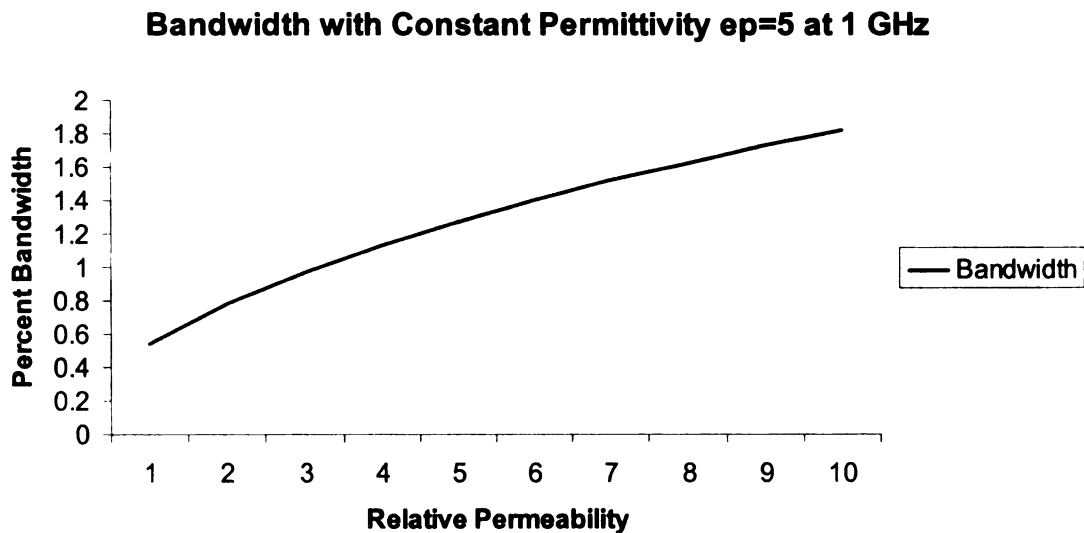


Figure 5.1.1: Bandwidth for constant permittivity with permeability varying from 1 to 10.

### Bandwidth with Constant Permeability $\mu=2$ at 1 GHz

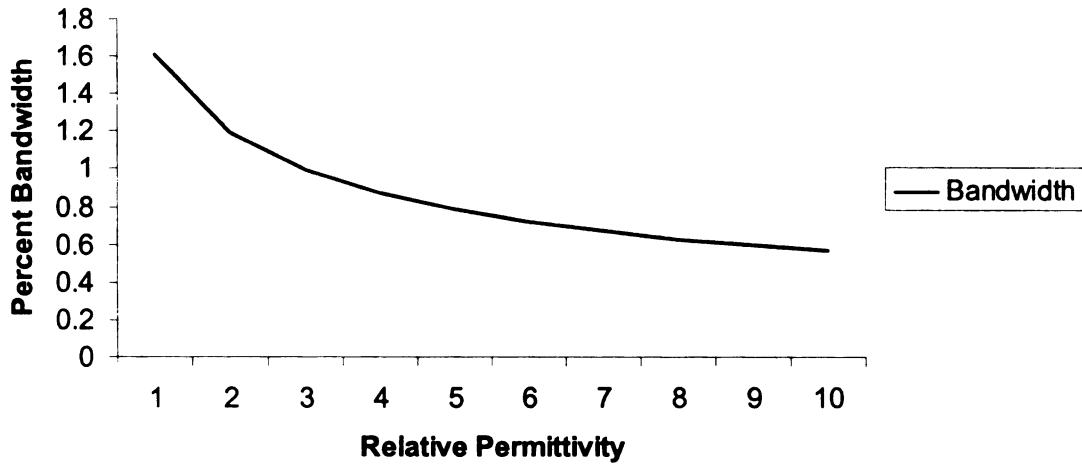


Figure 5.1.2: Bandwidth for constant permeability with permittivity varying from 1 to 10.

Using Sonnet Lite, a patch antenna with sides of length 4340 mils, approximately 110 mm, is simulated in order to determine the VSWR. The center frequency according to equation (5.1.1) is about 650 MHz, and the calculated bandwidth according to equation (5.1.4) is going to be 0.448%. The relative permeability and permittivity of the substrate are going to be almost equal in order to get the best matching. The values for permittivity and permeability are 2.2 and 2 respectively. Figure 5.1.3 shows the resulting VSWR graphed versus frequency.

In order to obtain the bandwidth from this graph, the lower frequency where VSWR=2 is subtracted from the higher frequency where VSWR=2 and the difference is divided by the center frequency. This gives a bandwidth of 0.46%, which is close the bandwidth found using equation (5.1.4).

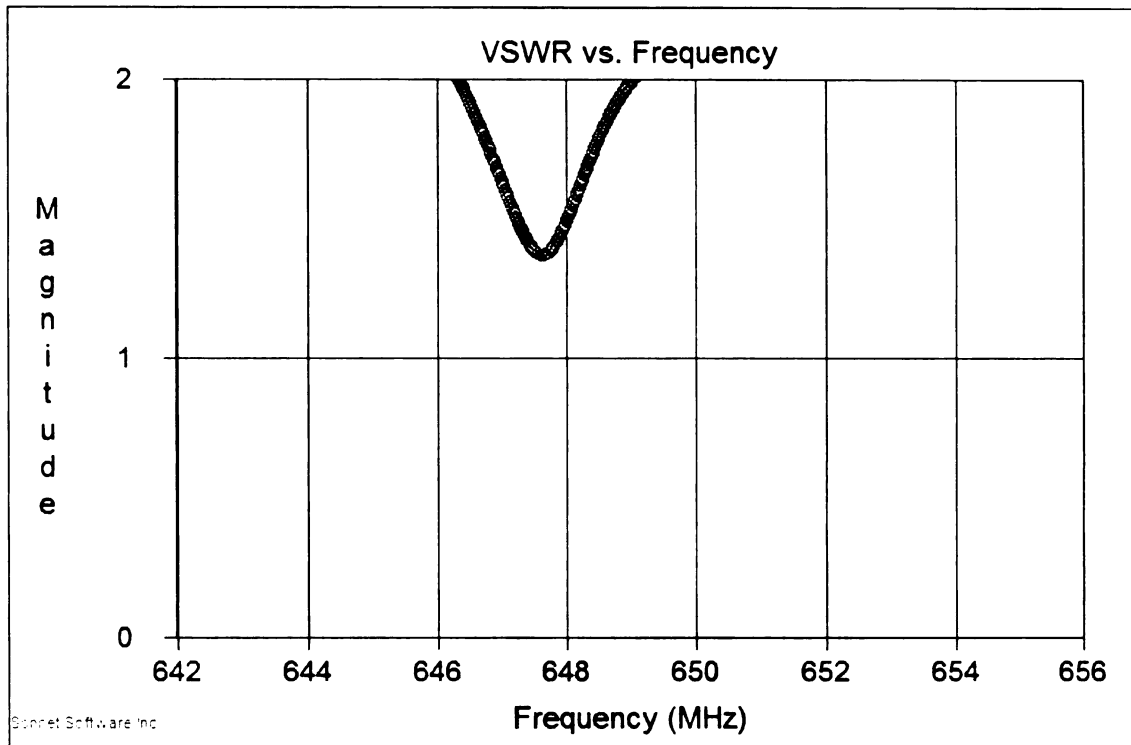


Figure 5.1.3: Bandwidth plot for permittivity of 2.2 and permeability of 2.

Now the data from the hexaferrite sample is used in equation (5.1.4) as well as the Sonnet Lite program for further comparison. The permittivity is 5.1 and the permeability is 1.5 which was obtained from the sample with volume fraction  $f=0.25$ . The bandwidth found by calculation is going to be 0.15% around a center frequency of 495 MHz. Figure 5.1.4 shows the VSWR graph using Sonnet Lite. The bandwidth found through this graph is 1.5%, which differs from the calculated amount by a factor of 10. This could be due to the fact that the equation predicts such a small bandwidth that it is not easily simulated using Sonnet Lite.

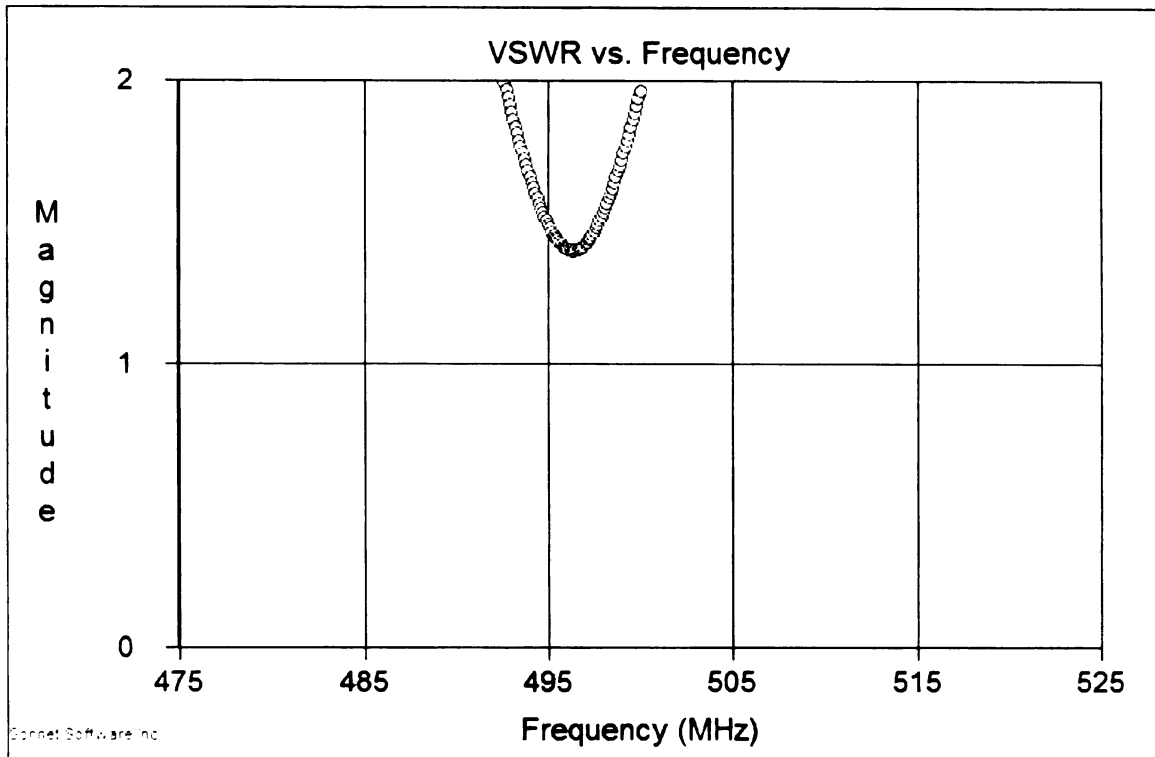


Figure 5.1.4: Bandwidth plot for permittivity of 5.1 and permeability of 1.5.

For aid in describing the benefit of using a magneto-dielectric material as the substrate as opposed to just a dielectric material, a non-magnetic material was modeled with this formulation and simulated with Sonnet lite. The patch antenna modeled is the same as seen above but with  $\mu_r = 1$  and  $\epsilon_r = 4.4$ , which results in a bandwidth percentage of only 0.22%. This is half the bandwidth percentage of the magneto dielectric material modeled in the first example. Sonnet-lite, however does not give the same bandwidth as the calculated results. The simulation actually shows an increase in bandwidth as seen in figure 5.1.5. This is an area that deserves attention in future work. The goal would be to setup an actual test procedure for getting real measured bandwidth results in order to determine if this formulation is an accurate prediction.

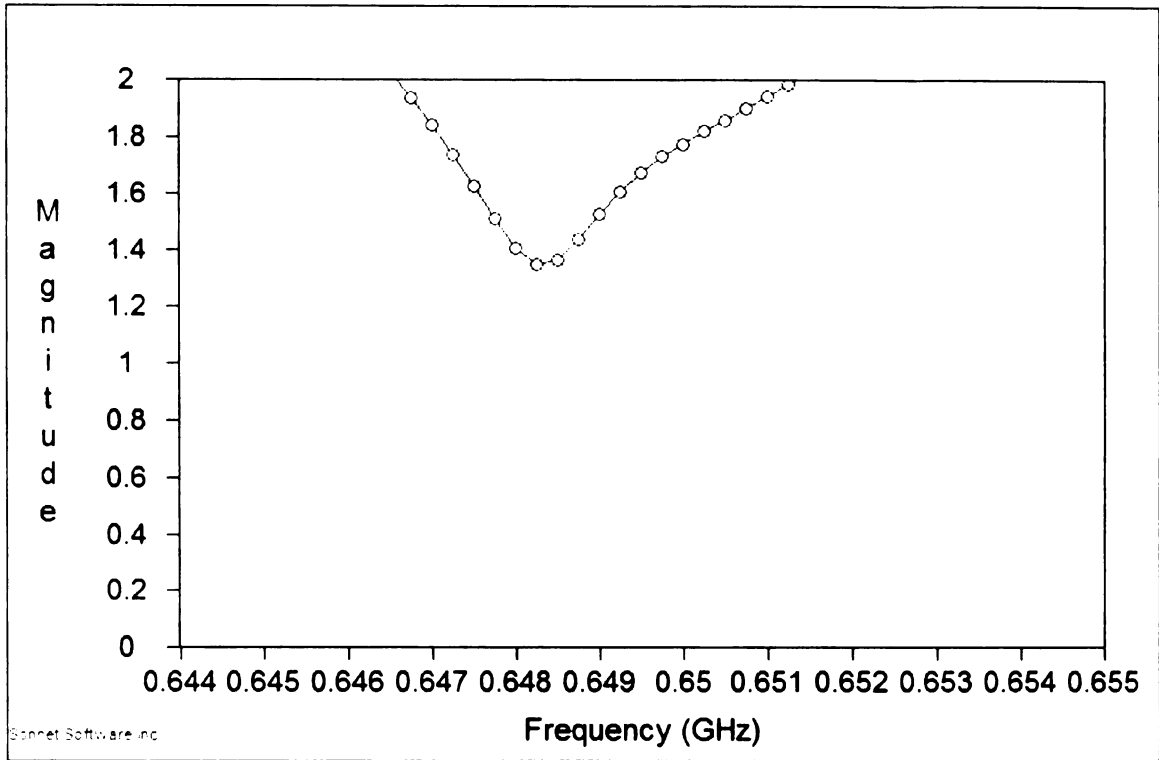


Figure 5.1.5: Bandwidth plot for permittivity of 4.4 and permeability of 1.

## **CHAPTER 6 – Conclusions and Future Work**

### **6.1 - Conclusion**

Upon comparing the results of the classical mixing formulas in this thesis compared to actual measured data, it can be seen that most of the permittivity models are relatively reliable. The Clausius Mosotti formula was shown that when used with a two phase mixture of spherical particles dispersed in an environment will give the same exact answer as the classical Maxwell-Garnett approach. These two mixing principles focus on the inclusions more than the background and how they affect the mixture; Maxwell-Garnett uses volume averaged field quantities, and Clausius Mosotti replaces the inclusions with polarizations. The other two formulations; Coherent Potential and Bruggeman's philosophy, attempt to homogenize the material and find the effective permittivity equally from the inclusions as from the environment based on their volume fractions. Of all four mixing equations, Coherent potential formulation is the most consistently accurate for all three volume fractions.

However, when applying the concept of duality and swapping the values of permeability for permittivity in these same equations they do not yield as good of results as when applied to permittivity. The Maxwell-Garnett formula gives much better results than other approaches, but is not accurate enough to be considered a reliable method for predicting permeability. As mentioned above, the Maxwell-Garnett and for this geometry Clausius Mosotti, focus more on the inclusions than on the environment. This was not as accurate for permittivity, but for permeability this does result in better data. When a magnetic inclusion is placed in a non-magnetic background the inclusion will have more control over the effective permeability and shows why these two formulations

will give better results than the homogenization approach used by Coherent Potential and Bruggeman. This shows that the magnetic behavior of heterogeneous materials is not easily predicted and it is necessary to analyze this problem on the quantum level for more precise results.

Another problem is the use of spherical particles as the inclusions. In order to maintain any of the magnetic properties of hexaferrite the volume fraction needed to be 0.4 or above. The problem with high volume fractions like this is that the weight of the mixture becomes not much less than if you had the hexaferrite in bulk. Figure 6.1.1 illustrates the correlation between volume fraction and weight fraction for density ratios of 10:1, 5:1, and 1:1.

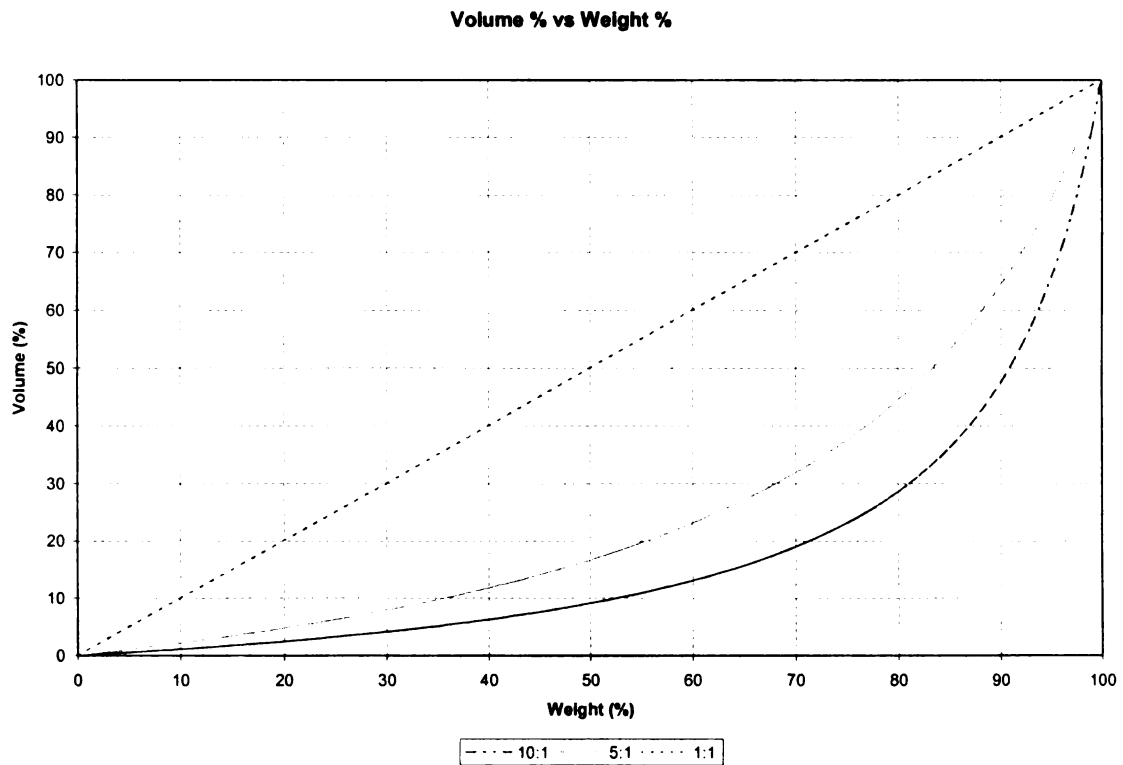


Figure 6.1.1: Comparison of volume percent to weight percent.

This ratio is the density of the inclusion to density of the environment. For a density ratio of 5:1, it can be seen from figure 6.1.1 that a volume fraction of 0.4, 40 % by volume, would become greater than 75% of the weight for that mixture. Also, as the volume fractions increases adjacent particles begin to interact with each other and can no longer be considered mono-domain which will increase the difficulty of predicting permeability and even permittivity. These results help to show that using spherical inclusions do not yield appreciable magnetic results and do not allow for a reduction in weight. As discussed in future work, other geometries will need to be considered in order to achieve better results.

## 6.2 - Future Work

Up to this point the only type of sample that was tested and was attempted to model have been C0D composites. This means that the mixture is conducting along 0 dimensions [1]. This consists of spherical particles dispersed in a polymer background and can be seen in Figure 6.2.1 along with the illustrations for C1D and C2D composites.

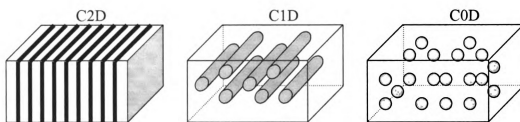


Figure 6.2.1: Types of composites.

In the future it might be beneficial to try the C1D or the C2D composites for two reasons. The first is for different results in the effective parameters based on their applications, and second reason is for accuracy of predicting the effective parameters. Another consideration is to use ferromagnetic materials; however these do not perform at as high of frequencies.

Also, if the COD composites are to still be used the modeling will have to be done on the quantum scale. Clearly the only way to fully predict the behavior of the magnetic properties of these mixtures will be to model the interaction and movement of electrons within a sample. Also, trying to compare the results of the mixing principles for other samples than can be measured will help to better understand the ability of these equations to predict permittivity and permeability and help realize their limitations.

Another aspect for future work is to setup a test procedure for the square patch antenna example. The test will be able to see the bandwidth results and allow us to compare them with the calculated results.

## BIBLIOGRAPHY

- [1] Acher, O., "Frequency Response of Engineering of Magnetic Composite Materials", *Advances in Electromagnetics of Complex Media and Metamaterials*. 39-59, 2003.
- [2] Böttcher, C.J.F., *Theory of Electric Polarization*, Elsevier Publishing Co.: New York, 1952.
- [3] Bruggeman, D.A.G., "Berechnung Verschiedener Physikalischer Konstanten von Heterogenen Substanzen", *Annalen der Physik*, **24**, 636-644, 1935.
- [4] Cheng, D.K., *Field and Wave Electromagnetics: Second Edition*. Addison-Wesley Publishing Company, Inc.: Reading, Massachusetts, 1989.
- [5] Gadenne, M., "Electromagnetic Response of Ferromagnetic Cermet: Superparamagnetic Transition", *Optical Properties of Nanostructured Random Media, Topics Appl. Phys.*, **82**, 249-273, 2002.
- [6] Gammon, D.C., *Electromagnetic Scattering Properties of Selected Magnetic Thin Films*, Masters Thesis: Air Force Instituted of Technology, 1989.
- [7] Hansen R.C., and Burke, M., "Antennas with Magneto-Dielectrics", *Microwave and Optical Technology Letters*, **26(2)**, 75-78, July 20 2000.
- [8] Infante, D.J., *Applications and Theory of Broadband Stripline Field Applicators*, Michigan State University: February 2000.
- [9] Isaacs, Alan, ed., *A Dictionary of Physics*. Oxford University Press: New York, 1996.
- [10] Ishimaru, A., *Electromagnetic Wave Propogation, Radiation, and Scattering*. New Jersey: Prentice Hall, 1991.
- [11] Kong, J.A., and Sihvola, A.H., "Effective permittivity of dielectric mixtures", *IEEE Transactions Geoscience Remote Sensing*, **26(4)**, 420-429, July 1988.
- [12] Lindell, I.V., and Sihvola, A.H., "Effective Permeability of Mixtures", *PIER 6: Progress in Electromagnetics Research: Dielectric Properties of Heterogeneous Materials*. New York: Elsevier Science Publishing Co., Inc., 1992.
- [13] Looyenga, H., "Dielectric constants of mixtures", *Physica*, **321**, 401-406, 1965.
- [14] Lord Rayleigh, "On the influence of obstacles arranged in rectangular order upon the properties of a medium", *Philosophical Magazine*, **32**, 481-502, 1892.

- [15] Maxwell, J.C., *A Treatise on Electricity and Magnetism*, 1,2 3<sup>rd</sup> ed. 1891, Dover Publication Inc., 1954.
- [16] Morrish, A.H., *The Physical Principles of Magnetism*. John Wiley & Sons, Inc.: New York, 1965.
- [17] Polder, D., and Van Santen, J.H., “The effective permeability of mixtures and solids”, *Physica XII*, 5, 257-271, 1946.
- [18] Rothwell, E.J., and Cloud, M.J., *Electromagnetics*. CRC Press: Boca Raton, 2001.
- [19] Sheng, P., and Gadenne, M., “Effective magnetic permeability of granular ferromagnetic metals”, *J. Phys.: Condens. Matter*, 4, 9735-9740, 1992.
- [20] Sihvola, A., *Electromagnetic mixing formulas and applications*. London: The Institution of Electrical Engineers, 1999.
- [21] Soohoo, R.F., *Theory and Application of Ferrites*. Prentice-Hall, Inc.: Englewood Cliffs, New Jersey, 1960.
- [22] Tinga, W.R., “Mixture Laws and Microwave-Material Interactions”, *PIER 6: Progress in Electromagnetics Research: Dielectric Properties of Heterogeneous Materials*. New York: Elsevier Science Publishing Co., Inc., 1992.
- [23] Wiener, O., *Abh. Math. Phys. Kl. Sachs Akad. Wiss.*, Leipzig, 32, 509, 1912.
- [24] Landau, L. and Lifshitz, *Electrodynamics of Continuous Media*. Pergamon: Oxford, 1960.
- [25] Kittel, *Introduction to Solid State Physics*. New York: John Wiley and Sons, Inc., 1986.
- [26] Tsang, L., Kong, J.A., and Shin, R.T., *Theory of Microwave Remote Sensing*. New York: Wiley, 1985.

MICHIGAN STATE UNIVERSITY LIBRARIES



3 1293 02511 0226